C. P. No. 595

C. P. No. 595

MINISTRY OF AVIATION

AERONAUTICAL RESEARCH COUNCIL

CURRENT PAPERS

On the Control of Shock-Induced Boundary-Layer Separation with Discrete Air Jets

By

R.A. Wallis, M.Eng.

of the Department of Supply, Australia

and

Mrs. C.M. Stuart, B.A.

of the Aerodynamics Division, N.P.L.

LONDON: HER MAJESTY'S STATIONERY OFFICE

1962

PRICE 7s.6d. NET

C.P. No.595

On the Control of Shock-Induced Boundary-Layer Separation with Discrete Air Jets

- By -
R. A. Wallis, M.Eng.
(of the Department of Supply, Australia)*
and
Mrs. C. M. Stuart, B.A.
(of the Aerodynamics Division, N.P.L.)

February, 1958

SUMMARY

High-speed tunnel experiments with discrete air jets possessing a spanwise ejection velocity component have shown that such jets produce a strong persistent vorticity similar to that associated with vane-type vortex generators. The use of small quantities of air facilitated the re-attachment of the separated layer downstream of the shock wave, whilst moderate quantities almost completely suppressed the separation. This work, which was of a preliminary nature, was carried out on a half-aerofoil fitted to the wall of the N.P.L. 9 in. × 3 in. high-speed wind tunnel.

Contents

6./

*On temporary service in the Aerodynamics Division, N.P.L.

Previously issued as A.R.C.19,865.
Published with the permission of the Director, N.P.L.

Notation

c	chord of bump
p	static pressure on surface
$p_{T.E.}$	static pressure on surface at trailing edge
q	mass flow in air jets/ft span
x	distance along chord from leading edge
x_{sh}	position of shock wave from leading edge
y	surface co-ordinate in vertical plane
C_Q	flow coefficient $\left(\frac{q}{\rho_o U_o c}\right)$
C_μ	momentum coefficient $\left(\frac{qV_j}{\frac{1}{2}\rho_o U_o^2 c}\right)$
M_o	free stream Mach number
H_o	stagnation pressure of tunnel air
U	local velocity on bump surface
U_o	free stream velocity
V_j	velocity of jet when expanded isentropically to local surface pressure
ρ_o	density of free-stream air.

1. Introduction

Discrete air jets have been successfully used in delaying turbulent boundary-layer separation at low speeds[1]. The jet arrangement employed consisted of a spanwise row of circular jets issuing into the airstream in a direction normal to the surface. The efficacy of such jets was assumed to arise from the increased mixing created by the induced vortices; these vortices are similar, in some respects, to those found downstream of counter-rotating vane-type vortex generators but lack the strength and persistency of the latter.

Considerable progress has been made recently in the development of vane-type generators as a means of controlling shock-

induced/

induced separation, (e.g., see Ref. 2). This success, therefore, encouraged the belief, first expressed in Ref. 1, that discrete air jets could be developed to exercise a similar control.

As a preliminary to the high-speed tests described herein, low-speed tests were conducted for the purpose of developing an air jet capable of producing a strong, persistent type of vorticity[3]. Jets which issued from the surface with a spanwise velocity component produced vorticity of the desired type, and hence were considered superior to the normal-to-surface jets used in the low-speed applications[1].

High-speed tests to check the effectiveness of the inclined jet were carried out during May and June, 1956 in the 9 in. × 3 in. high-speed wind tunnel at the N.P.L. The model, which consisted of a half-aerofoil forming a bump on a 3 in. wall of the tunnel, was similar to that used previously for tests with vane-type vortex generators[2].

2. Scope of Tests

The primary purpose of these tests was to check the usefulness of air jets in delaying separation without undertaking a comprehensive study of the possible variables. A list of the main parameters is now given, and is followed by a short discussion on the approach to each of them.

(a) Shape of test surface

(b) Chordwise location of air jets

(c) Sense of vortices, i.e., counter-rotating or co-rotating

(d) Inclination of jets to chordwise and spanwise planes of reference

(e) Spacing of jets, i.e., pitch

(f) Diameter of efflux hole

(g) Jet efflux velocity (or box pressure)

(h) Wind-tunnel Mach number.

(a) Tests were first carried out on a half-aerofoil, or 'bump', for which the shock-induced separations were not very severe. Air jets proved successful in controlling these and hence the bump was modified to give a more adverse condition; most of the work relates to this latter arrangement.

(b) Single rows of air jets were provided at two chordwise positions. With one exception, these were operated independently of each other in order to provide information on a number of points as follows: the shock wave, which develops with increasing Mach number, is first apparent at a position between the two rows. With the upstream row of jets operating, the persistency of the vorticity can be gauged from the change in the effectiveness of the device as the shock wave moves away from the holes towards the trailing edge with increasing Mach number. Shock-induced separation commences for shock positions upstream of the second row of jets, and it is therefore possible with this row of jets alone to check the effect of jets issuing into a region of separation. Finally, a comparison, for far

back/

back shock positions, of the results obtained with the upstream row of jets with those for the second row, permits a qualitative check on the rate at which the effective vorticity diminishes.

(c) Based on the experience gained with vane-type vortex generators (see Ref. 2, for example), only co-rotating vortex arrangements were used as these appear to be the most effective type for covering a wide range of operating conditions.

(d) A limited, unpublished, investigation in a low-speed wind tunnel suggested that modifications to the jet inclination used in Ref. 3 were unlikely to produce first order improvements. The arrangement of Ref. 3 was therefore adopted; it is not suggested that this necessarily represents the optimum configuration, but time did not permit a more detailed investigation.

(e) It is known that as the pitch of co-rotating vortex generators is increased their effectiveness rises rapidly to an optimum, and then falls slowly. With this fact in mind, the pitch of the air jets for the present tests was derived from the data of Refs. 2 and 3, keeping on the high side of the optimum in order to be safe.

(f) and (g) A number of hole sizes and blowing pressures were investigated in an attempt to determine whether the mass-flow coefficient of the jets, or the momentum coefficient, is the more important variable.

(h) Shock position and hence, because the bump is curved, shock strength, were varied by varying the tunnel Mach number; transonic liners were not fitted.

3. Experimental Details

3.1 Model installation

The basic model was a 6% thick half-aerofoil defined by Tanner's general equation[4]

$$\frac{y}{c} = a\frac{x}{c}\left\{1 - \left(\frac{x}{c}\right)^{n}\right\}, \qquad \ldots(1)$$

with $a = 0.127$, $n = 3$ and the origin at the trailing edge.

In order to increase the severity of the shock-induced separation, the thickness was increased to 8% by tilting the model about the trailing edge as shown in Fig. 1, and then adding a fairing at the leading edge. As shown in Ref. 4, the new profile is represented by equation (1) with the value of a increased by the tangent of the angle of tilt, i.e., with a increased to 0.169. These two shapes are identical to the ones employed by Tanner and Pearcey[2]. The chord of the basic model was 6 in.; the modifications increased this to 6.6 in.

The turbulent boundary layer on the wall ahead of the bump was thinned by means of a suction arrangement shown in Fig. 2. A series of transverse slits led into a suction box which in turn was connected to a large capacity suction pump.

Small-bore,/

Small-bore, flush surface static tubes were fitted at $\frac{1}{4}$ in. chordwise intervals. These were located on the mid-span position and no attempt was made to explore the small spanwise variations of pressure through the vortices created by the jets. Surface pressure tubes were also provided along the mid-span position of the tunnel wall downstream of the model.

The model spanned the 3 in. width of the tunnel, and thin rubber sheet was used as a seal between the ends of the model and the glass walls. Similarly, rubber was used to seal all tunnel wall joints.

3.2 Air-supply details

Air was bled from the high pressure supply to the tunnel, and passed through an orifice-plate flow meter before reaching the bump. The supply "box" for each row of jets consisted of a $\frac{3}{8}$ in. diameter hole drilled through the model in a spanwise direction and sealed at the ends. The supply air was fed to each box at two positions by means of $\frac{3}{8}$ in. internal diameter tubes (Fig. 2). "Sealing" at the inoperative chordwise station was achieved by short circuiting the two inlet tubes with a piece of rubber hose.

The two rows of air jets were drilled at 3.6 in. and 2 in. from the trailing edge of the bump. Hence, for the 6% thick bump the jets were at 40% and 66.7% of the chord, respectively, from the leading edge, and at 45.5% and 69.7% chord for the 8% thick bump.

Each row of holes was at right angles to the free-stream direction. The holes were drilled, in a plane normal to the surface, to make an angle of 45° to the surface. The distance between the hole at the end of a row and the respective side wall was made different on the two sides to allow to some extent for the spanwise movement of the vortex pattern downstream of the jets (see Ref. 3). Thus, commencing at the wall towards which the jets were blowing, the distance between the wall and the first jet was made equal to the pitch of the jets, namely 0.31 in. This left a distance of 0.21 in. between the last hole and the other wall.

The air-supply equipment was designed to allow the use of "box" pressures up to 100 p.s.i. in excess of atmospheric pressure. Since the tunnel stagnation pressure was approximately equal to atmospheric pressure, the pressures read on Bourdon gauges were taken as being the excess over stagnation pressure.

3.3 Experimental techniques

The present tests followed very similar lines to those described in Refs. 2 and 5 and hence full use has been made of the experience gained in these earlier experiments. The downstream movement of the shock wave with increasing Mach number is of prime importance; it has been found from previous tests that the shock-wave position is best controlled when using a static pressure near the trailing edge as a reference level. In these tests the static pressure $\frac{1}{4}$ in. upstream of the trailing edge was chosen.

For arbitrarily chosen reference pressures, a set of pressure distributions were obtained which covered the Mach number range of the tests for a given configuration. Schlieren photographs to match these test conditions were obtained at a later period. For simplicity, the gauge reading of the air-jet box pressure was kept constant through the entire speed range instead of being adjusted with speed to keep C_Q constant.

Surface/

Surface flow patterns were obtained using a mixture of titanium oxide and oil smeared over the blackened surface of the model. With the tunnel running, 35 mm photographs were taken, through the side wall, when the patterns were considered suitably developed; this technique was not used in Refs. 2 and 5.

Before commencing the main tests, boundary-layer traverses were taken 2 in. downstream of the leading edge. The suction arrangement was progressively improved until with full suction the boundary-layer thickness at this point had been reduced to approximately 0.08 in.; this was considered satisfactory.

4. Results

4.1 6% thick bump

The experimental work on this model was done in two stages. In the first, only the forward row of holes was drilled and these holes originally had a diameter of 0.020 in. A definite improvement was obtained with these jets but it was thought that the holes were probably well below the optimum size. As a consequence, the holes were opened up to 0.031 in. diameter and the second row of holes added at this stage. The results obtained were very encouraging and in order to provide a more severe test for the jets, the thicker bump was later installed for a more complete survey of the effect of hole size.

In order to keep the number of illustrations to reasonable proportions, the results for the 0.020 in. dia. holes have been omitted and selected cases chosen for the 0.031 in. dia. configurations.

4.1.1 Pressure distributions

The chordwise distributions of pressures are given in Figs. 3 to 6 for a number of blowing pressures. Each curve corresponds to a separate Mach number; as the tunnel speed is increased, the shock moves downstream until the tunnel chokes with the shock just upstream of the trailing edge. It will be noted that, at the higher Mach numbers, the curve upstream of the shock is a unique one. This is now a well known feature of transonic flow over aerofoils and is often referred to as the "Mach number freeze"[6].

The first effect of blowing is to increase the rate of pressure recovery downstream of the shock (see Figs. 3 and 4). With increasing air-jet strength, the pressure rise through the shock becomes larger (see Figs. 5 and 6). Further increases in blowing pressure make very little difference.

Pressure distributions for a given trailing-edge pressure and varying air quantities are given in Fig. 8. For this trailing-edge pressure there is first a substantial downstream movement of the shock with increasing jet flow, followed eventually by a tendency to move forward again. This may be due to an excessive thickening of the boundary layer or to a less favourable arrangement of the vortices.

The foregoing relates to results for air jets in the forward location. Only one set of pressure distributions is shown for the rear position (Fig. 7) and this is for the optimum blowing pressure. Due to the closer proximity of the jets, the pressure rise through the shock is greater for shock waves nearing the trailing edge than that obtained with the configuration of Fig. 6.

Superimposed on Figs. 6 and 7 are curves for a co-rotating vane-type vortex generator arrangement used in Ref. 2. These were located further forwards than the air jets and hence are not strictly comparable. Counter-rotating arrangements which were used nearer the shocks[2] gave better results than the co-rotating ones shown but were not as effective as the air jets.

4.1.2/

4.1.2 Schlieren photographs

The preceding results are supplemented with the schlieren photographs of Figs. 9 to 13, for which the cut-off was arranged to show the boundary layer as a dark feature. Each of Figs. 9 to 12 consists of a set of photographs illustrating the effect of increasing Mach number for a fixed blowing condition. Fig. 13 shows the effect of increasing blowing pressure for a fixed trailing-edge pressure.

As mentioned previously, separation is never very severe on this bump, even in the absence of any boundary-layer control. In Fig. 9 (a), the shock is normal to the surface thus signifying the absence of separation; the boundary layer can be seen to thicken appreciably as the trailing edge is approached.

It helps in interpreting the schlieren photographs to remember that, with the cut-off arrangement used here, the boundary layer appears blackest in the region of greatest density gradient, and hence approximately in the region of greatest gradient in the boundary-layer velocity profile. Thus, in Fig. 9 (a), the black boundary layer is indistinguishable from the black shadow of the surface until it has reached a fair thickness and the velocity gradient at the surface itself has begun to fall.

Shock-induced separation is evidenced by the deflection of the black boundary layer away from the surface through an appreciable angle. Downstream of separation, the shear layer spreads fairly rapidly and its edges become irregular. The central part of this layer, where the density gradients are greatest, appears as a black tongue. The 'dead air' between the shear layer and the surface has approximately the same shade as the background. Under the influence of fluid mixing and the associated pressure rise, the shear layer spreads and also bends back towards the surface[7]. However, it is often difficult to decide from the photographs just where the layer re-attaches to the surface. For the set of photographs without blowing, Fig. 9, it seems fairly safe to deduce that re-attachment does not occur upstream of the trailing edge for Fig. 9 (d) or Fig. 9 (e) and that it occurs between the shock and trailing edge for Fig. 9 (b); for Fig. 9 (c), one cannot be more definite than to suggest that re-attachment probably occurs just upstream of the trailing edge. In many cases with blowing, the mixing is artificially enhanced by the vortices and the re-attachment process thereby accelerated. From the schlieren photographs, the degree of separation present in any particular case must be interpreted in the light of experience.

A feature of the main shock wave that is almost invariably indicative of separation is the straight, 'toe'-like portion of the foot, meeting the surface obliquely.* The angle of this oblique part to the surface provides some indication of the strength of the pressure rise through the shock at the surface, and its extent above the surface seems to bear some relation to the extent of the separation.

The progressive movement of the shock wave with increasing Mach number can be followed in Figs. 9 (a) to 9 (f). The separations appear more severe in Figs. 9 (d) and (e) and this is confirmed in the pressure distributions of Fig. 3, where there is a noticeable reduction in the pressure gradient downstream of the shock.

The/

*This only applies, of course, when the shock meets the surface upstream of the trailing edge, because the shock always becomes oblique once it has reached the trailing edge, even if separation is not present.

The use of air bled from the box at stagnation pressure (Fig. 10), produces improvements which are evident when attention is paid to the features described above. Compression and expansion waves in the vicinity of the jets do not appear to be of any consequence to events downstream of the main shock. The vorticity created downstream of the jets is evident on the photographic plates but is relatively small, and hence is not visible on the reproductions.

An increase of blowing pressure up to the optimum (Fig. 11) gives improvements that are readily apparent. The presence and extent of the vorticity created by the jets is now obvious as a black streak above the surface.

Since the most intense shock-induced separations occur fairly well back on the bump, a more rearward location of the jets might be expected to be advantageous. This is supported by the further improvement shown in Fig. 12. The 'lambda' foot of the shock is now almost entirely confined to the region of vortex flow and hence suggests an almost immediate re-attachment of the shear layer.

Finally, the photographs corresponding to the pressure distributions of Fig. 8 are presented in Fig. 13. The progressive suppression of separation with increasing blowing pressure is self-evident, at least up to 40 p.s.i. However, the forward movement of the shock for 60 p.s.i. (see Fig. 13 (d) and (e) and Fig. 8) can be clearly seen, and it may be significant that for this case the vortices from the jets seem to have moved further away from the surface than before, where they would be less effective.

4.2 8% thick bump

The presentation of detailed data will be confined almost entirely to one hole size, namely 0.035 in. diam., because there is a marked similarity between the results for different hole sizes. The overall effects of the other configurations will be discussed in Section 6.

4.2.1 Pressure distributions

Results for a number of air-jet arrangements are presented in Figs. 14 to 21. For the case of the plain bump (Fig. 14) the effects of separation are well in evidence. With increasing test Mach number, a stage is reached where the shock remains relatively stationary as the severity of the separation increases. This is followed by a very rapid movement up to the point of tunnel choking.

The general comments concerning the effect of increasing jet flow, which were made in Section 4.1.1, hold for Figs. 15 to 20.

Limited tests were carried out on an arrangement where both rows of jets were simultaneously active. A preliminary check suggested that a pressure of 20 p.s.i. was close to optimum and hence the work was confined to this pressure (Fig. 21). Shock-wave strength appears to be well maintained throughout the whole Mach number range.

Although there was no large significant difference between the results for various hole sizes it was decided to compare distributions for the best upstream and downstream arrangements with those for co-rotating vane-type vortex generators[2] situated at the same position as the forward jets (Figs. 22 and 23).

The effect of blowing pressure on shock position for a given trailing-edge pressure is illustrated in Fig. 24. Because of the

more/

more severe initial separation the comparison between the air-jet and plain bump cases is more striking than in Fig. 8.

4.2.2 Schlieren photographs

Flow conditions for a range of air-jet configurations are illustrated in Figs. 25 to 30.

Separation in the absence of boundary-layer control is very severe (Fig. 25).

When studying the results for air-jet arrangements, due allowance must be made for the separation due to side-wall effects. These effects will be discussed more fully in Section 5. Although the schlieren equipment was focussed on the flow near the centre line of the tunnel, flow details of the end separations have unavoidably been superimposed. Attention should be paid to the black "tongue" mentioned previously when assessing the effect of the air jets on separation.

The effectiveness of the air jets appears to have been maintained in this more severe case of the 8% bump.

Photographs for the flow conditions given in Fig. 24 are presented in Fig. 30 and illustrate, for a given trailing-edge pressure, the progressive suppression of the separation with increasing jet flow.

5. Wind-Tunnel Wall Effects

The conduct of so-called two-dimensional tests on any model spanning a wind tunnel becomes very difficult when boundary-layer control is attempted in regions of severe adverse pressure gradient. In low-speed testing, devices can be employed to minimise the effects of thick boundary layers on the side walls, and possibly also of unwanted separation there, but in high-speed tests of this kind very little can be done if schlieren photographs are required. Thus, because the side walls are of glass it is not possible to remove the boundary layer upstream of the model nor to extend the air-jet configuration to these walls. As a consequence, the severity of the separation is greater at the model extremities than elsewhere. The usual secondary flows associated with these conditions tend to spread this severe separation inboard.

A surface flow technique, described in Section 3.3, has been used in an attempt to assess the influence of the side walls in the present tests. Fig. 31 shows typical cases for the 8% bump: (a) in the plain condition, (b) with downstream jets issuing into a region of separation, and (c) with upstream jets active. The inclined jets have their cross-flow component in the direction of the side more seriously affected by wall boundary layers. The narrow streaks downstream of inoperative holes are mainly due to the fact that the fluid from upstream that would normally have moved along to replenish the fluid scrubbed from these regions, runs down into the holes, under gravity, instead.

Figs. 31 (b) and (c) are for blowing pressures equal to stagnation pressure. With increasing pressures the large, end separations are progressively reduced in spanwise extent but never eliminated. It is not surprising that these separations should make themselves evident in the schlieren photographs. The effect on the measured pressure distributions is not known but, since the tests are mainly comparative and the central flow is representative of the flow changes produced by the jets, the results are acceptable. Any

attempt/

attempt to read too much into them should, however, be discouraged. In conclusion it should probably be emphasized that the flow directions indicated in Fig. 31 are surface ones; small distances above the surface the directions would be rapidly approaching those of the undisturbed flow.

6. Analysis

6.1 Method adopted

At high subsonic speed, the lift potential of an aircraft is often limited by the severe buffeting and other adverse effects that accompany shock-induced separations. These effects have been shown to commence when, for a given incidence, the trailing-edge pressure versus Mach number curve suddenly changes slope with increasing speed[7]; the phenomenon has become known as the trailing-edge pressure divergence. It was also shown in Ref. 7 that the irregularities in the movement of the shock wave as a function of trailing-edge pressure were useful alternative indicators of separation effects. This was the basis of the method of analysis used exclusively in Refs. 2 and 5 and which will be adopted for the present tests.

It was demonstrated in Ref. 7 that the flow over one surface (usually the upper surface) of any given aerofoil could be considered in isolation in terms of the shock position and the trailing-edge pressure, and that, this far, there was no difference between the isolated surface and the surface of a half-aerofoil on a tunnel wall considered in the same way. However, in order to fit the flow over the isolated surface into the overall flow for the complete aerofoil, i.e., to fit it to the flow on the opposite surface and to the free-stream Mach number, certain conditions had to be satisfied by the trailing-edge pressure. These conditions are likely to be different for the complete aerofoil and the half-aerofoil, and so any comparisons that are made between the two cases have to be confined to the flow on the curved surface for given trailing-edge pressures.

With decreasing trailing-edge pressure, which follows in practice from increasing Mach number, the shock wave moves downstream over the curved surface in a regular manner provided separation is absent. When separation occurs it restricts the pressure rise through the shock and severely reduces the rate of pressure recovery downstream of the shock. The distance required for the pressure to rise from that just upstream of the shock to a given trailing-edge value will therefore be greater than in the absence of separation. In other words, if separation is present the shock is further forward than it should be; or again, the further back the shock is, the more efficient is the pressure recovery. This approach is analogous to thinking of the bump as one wall of a supersonic nozzle where the position of the normal shock for a given exit pressure will depend on the pressure recovery through the shock and along the nozzle. Separation or thickening boundary layers affect this pressure recovery and cause the shock to move forward at a given exit pressure. When the system has the most efficient boundary-layer control arrangement, the shock will be in the most downstream position.

An additional argument for the use of the above method of analysis is the high degree of consistency obtained with all results. The three-dimensional effects noted in Section 5 do not appear to invalidate comparative results of this nature although they would most certainly impair direct comparisons between these tests and those on actual aerofoils, in terms of free-stream Mach number particularly. Wall separations and lack of a free wake downstream of the "trailing edge" will produce first order modifications in the value of the trailing-edge pressure and so prevent the desired correlation.

6.2/

6.2 Shock-wave movement

The position of the shock wave has been taken arbitrarily as the point at which a tangent to the upstream pressure distribution intersects an extension of the linear pressure rise through the shock. Trailing-edge pressures have been obtained by interpolation since no pressure tube was provided at the exact position.

The shock movement curves for the 6% bump are presented in Fig. 32. The curve for no blowing shows the characteristic slowing up in shock movement when separation first occurs, with the shock at about 0.6 chord. The movement accelerates again once the pressure recovery has fallen to a minimum (see Fig. 3). For the most efficient air-jet arrangement, the movement is roughly linear until the shock reaches approximately 0.8 chord and then, for low trailing-edge pressures, the slope decreases as the shock approaches the trailing edge. In order to understand the reason for this reduction of slope, and hence fall in effectiveness, it must be appreciated that devices such as this, and co-rotating vane-type vortex generators, do not always completely eliminate the separation. They rely for their effectiveness, or for their overall improvement in pressure recovery, partly on the increased pressure rise up to separation (i.e., through the shock) and partly on the pressure rise associated with the re-attachment which they induce immediately following separation. (The pressure rise through the shock is not the complete amount that would be expected in the absence of separation, but this defect is compensated for by a rate of recovery downstream of the shock that is greater than would be expected in the absence of separation.) Provided there is sufficient of the chord between separation and the trailing edge for this process to be complete, the result is usually just as favourable as it would be if separation were completely suppressed. However, as the shock, and hence the separation position, approach the trailing edge, the benefit from the increased pressure recovery associated with re-attachment tends to diminish and so the effectiveness of the devices tends to fall off. For the present case, this may be aggravated by the side-wall effects, and it would also be less apparent if the results were analysed in terms of Mach number instead of trailing-edge pressure.

Intermediate between the best air-jet arrangement and the plain bump cases just described, are the results for the other air-jet configurations. In view of the test conditions, however, too much should not be read into small local changes of slope.

Similar results for the 8% bump are presented in Figs. 33 to 35 for three different hole sizes. The same general comments apply with the exception that, for the downstream row of jets, the sudden movement of the shock occurs when the shock passes the air-jet station. Neglecting the important three-dimensional effects in a case such as this, it can be said that the rapid movement is due to a change in the jet effectiveness. When the boundary layer separates upstream of the jets, the boundary layer losses are appreciable despite the fact that the jets re-attach the layer immediately downstream. In contrast, the injection of air upstream of the shock wave tends to suppress separation with a subsequently thinner boundary layer.

From the above, therefore, it is clear that the shock movement form of presentation is a yardstick by which the relative efficiency of any particular configuration can be judged. Unfortunately, however, it does not provide a measure of the extent to which the severity of buffeting is suppressed in a particular case although there must be a correlation with the above analysis. This was certainly found to be the case for vane-type vortex generators.

Moreover,/

Moreover, since there has now been considerable experience in the use of co-rotating vortex generators to delay buffeting in flight, a useful indication of the likely effectiveness of air jets in practice can be obtained from the comparisons of the present results with the corresponding ones for co-rotating vane-type generators.

6.3 Air jet parameters

The mass-flow coefficient used in Ref. 5 has been adopted. This is,

$$C_Q = \frac{q}{\rho_0 U_0 c}.$$

During the experimental work it was found convenient to hold the box pressure constant over the operating Mach number range and since the surface pressure near the jets remained sensibly the same, constant mass flow in the jets resulted. Hence it follows from the above definition that C_Q is changing as the Mach number is increased. In the induced flow tunnel used, however, ρ_0 falls as U_0 increases and this restricts the variation of C_Q. Since a coefficient of the above form has obvious limitations from a fundamental point of view, an approximate estimate appeared to be in order. Therefore, it has been assumed that $M_0 = 0.90$ and the values of C_Q so obtained have been plotted in Fig. 36 as a function of box pressure. On reference to Figs. 33, 34 and 35 it can be seen that values as low as 0.0002 have a marked effect and that values of 0.001 are extremely effective.

Another parameter of some interest is the ratio between the jet velocity and the local velocity. On the assumption that the air expands isentropically from the box pressure to the local free stream pressure, Fig. 37 has been prepared. The values so obtained do not appear unreasonable and very little difficulty should be experienced, in practice, in obtaining such ratios.

In Ref. 5 a momentum coefficient of the following form was evolved, namely,

$$C_\mu = \frac{qV_j}{\frac{1}{2}\rho_0 U_0^2 c},$$

or alternatively

$$C_\mu = C_Q \cdot \frac{2V_j}{U_0}.$$

Hence, the procedure of presenting C_Q and V_J/U as the relevant air-jet parameters is equivalent to adopting some form of momentum coefficient.

A rigorous analysis of the results, for the purpose of attempting correlation of the data in terms of some suitable parameter, was discouraged in view of the experimental limitations mentioned previously.

6.4 Air jet location

Air jets are most effective when they are situated just upstream of the shock-wave position. However, provided the shock wave is not more than 30% to 40% c downstream of the jets, separation is

very/

very effectively controlled. The persistency of the vorticity ensures large improvements even when the shock wave has moved still further downstream of the jets.

On comparing the results of Ref. 2 with the present work, vane-type vortex generators do not appear to be as effective as air jets when the shock is just downstream of the device location. The reason for this is not known but it may be associated with the wakes shed from the vanes. From oil flow patterns and general observations there do not appear to be any regions of low energy air in the neighbourhood of air jets.

The ability of air jets to re-attach the boundary layer when they are discharged into a region of separated flow may be useful in practice. It will mean that they will not necessarily have to be located upstream of the most forward separation position likely to be encountered within the flight envelope, and that they can therefore be placed further back on the chord than vane-type generators would be and so maintain a greater effectiveness when the shock is approaching the trailing edge at high Mach numbers.

6.5 Reynolds number effects

At a free-stream Mach number of 0.9 the Reynolds number of the present tests is approximately 2×10^6. Since the wind tunnel is unpressurised, no tests would be carried out with varying Reynolds number. Any attempt to estimate the effect of Reynolds number on the air-jet parameters must therefore be pure speculation. Nevertheless, the authors believe that marked decreases in C_Q might be expected as the ratio of inertia to viscous forces increases, i.e., as the Reynolds number is increased. Tests at higher Reynolds numbers, either in a wind tunnel or flight, are indicated.

7. Acknowledgements

The author wishes to acknowledge the support and advice received from Mr. H. H. Pearcey and also the assistance rendered by Mr. A. Chinneck in the early stages of the work.

References/

References

No.	Author(s)	Title, etc.
1	R. A. Wallis	The use of air jets for boundary layer control. A.R.L. (Melb.) Aero Note 110. June, 1952.
2*	L. H. Tanner and H. H. Pearcey	The effects of vortex generators on a shock-induced turbulent boundary layer separation on a curved surface. (In preparation.)
3	R. A. Wallis	A preliminary note on a modified type of air jet for boundary layer control. A.R.C. C.P.513. May, 1956.
4	L. H. Tanner	Curves suitable for families of aerofoils with variable maximum thickness position, nose radius, camber and nose droop. A.R.C. C.P.358. February, 1957.
5	A. Chinneck, Miss G. C. A. Jones and Miss C. M. Tracy	An interim report on the use of blowing to reduce the fall in control effectiveness associated with shock-induced separation at transonic speeds. A.R.C.17,564. April, 1955.
6	C. S. Sinnott	On the flow of a sonic stream past an aerofoil surface leading to a semi-empirical method for the prediction of sonic-range pressure distributions. J. Aero/Space Sci., Vol.26, No.3. March, 1959.
7	H. H. Pearcey	Some effects of shock-induced separation of turbulent boundary layers in transonic flow past aerofoils. Paper No.9 presented at the Symposium on Boundary Layer Effects in Aerodynamics at the N.P.L., Teddington, Middlesex, 31st March - 2nd April, 1955. A.R.C. R. & M.3108. June, 1955.

---

*This paper was never prepared. However, most of the subject matter is contained in:

H. H. Pearcey — Shock-induced separation and its prevention by design and boundary layer control. (Section 4.5.) Boundary Layer and Flow Control. Pergamon Press, Vol.2, pp.1277-1312. 1961.

WS

FIG. 1.

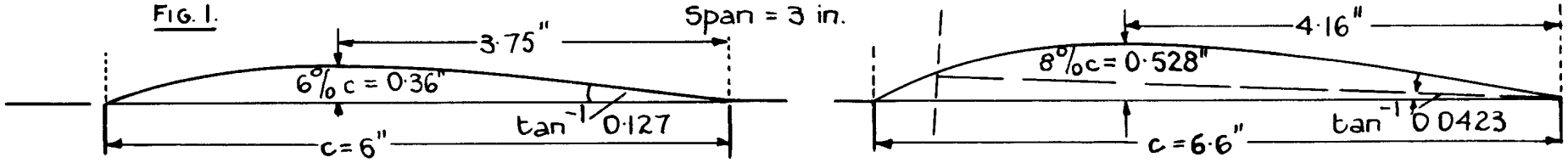

Diagram of 6% and 8% bumps

FIG 2.

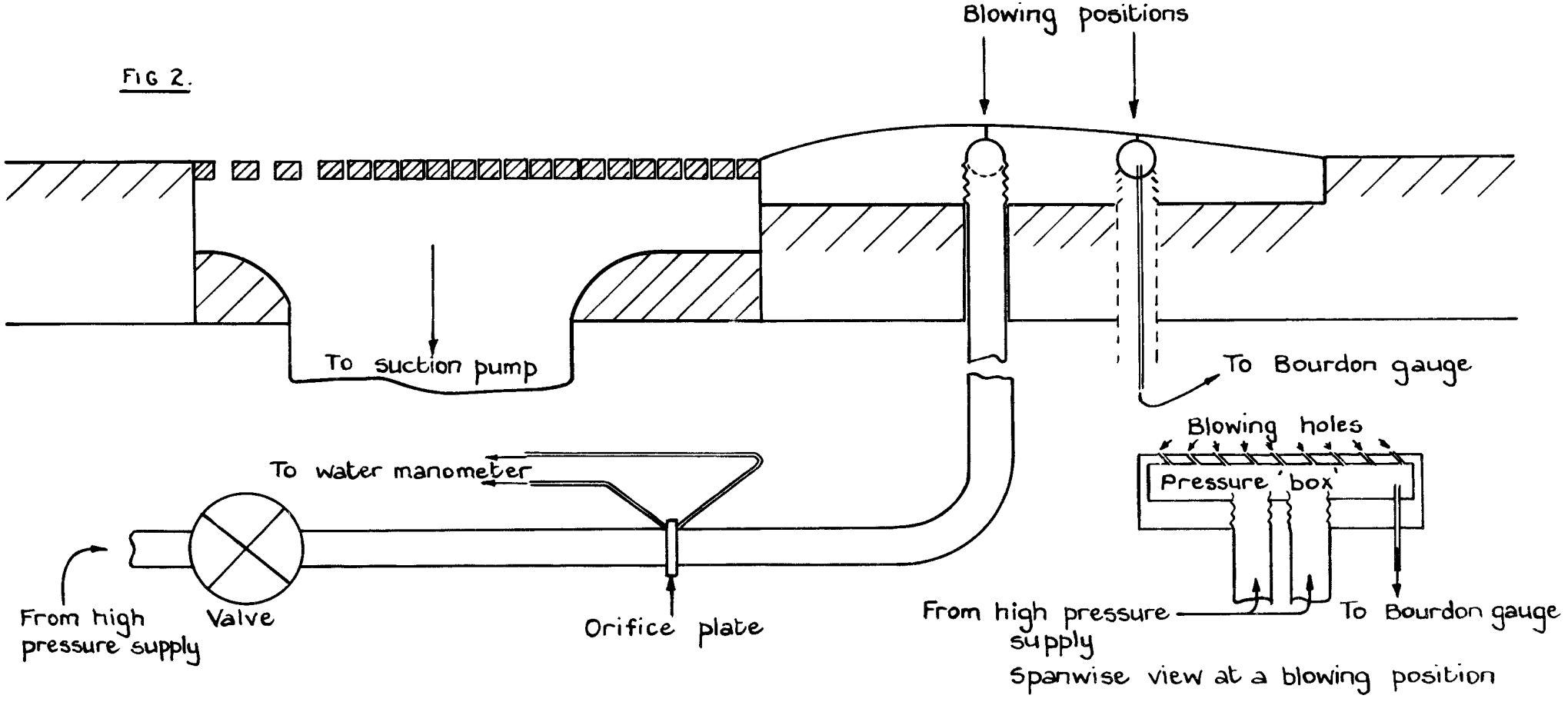

Diagram of arrangement of a bump.

FIG 1 & 2

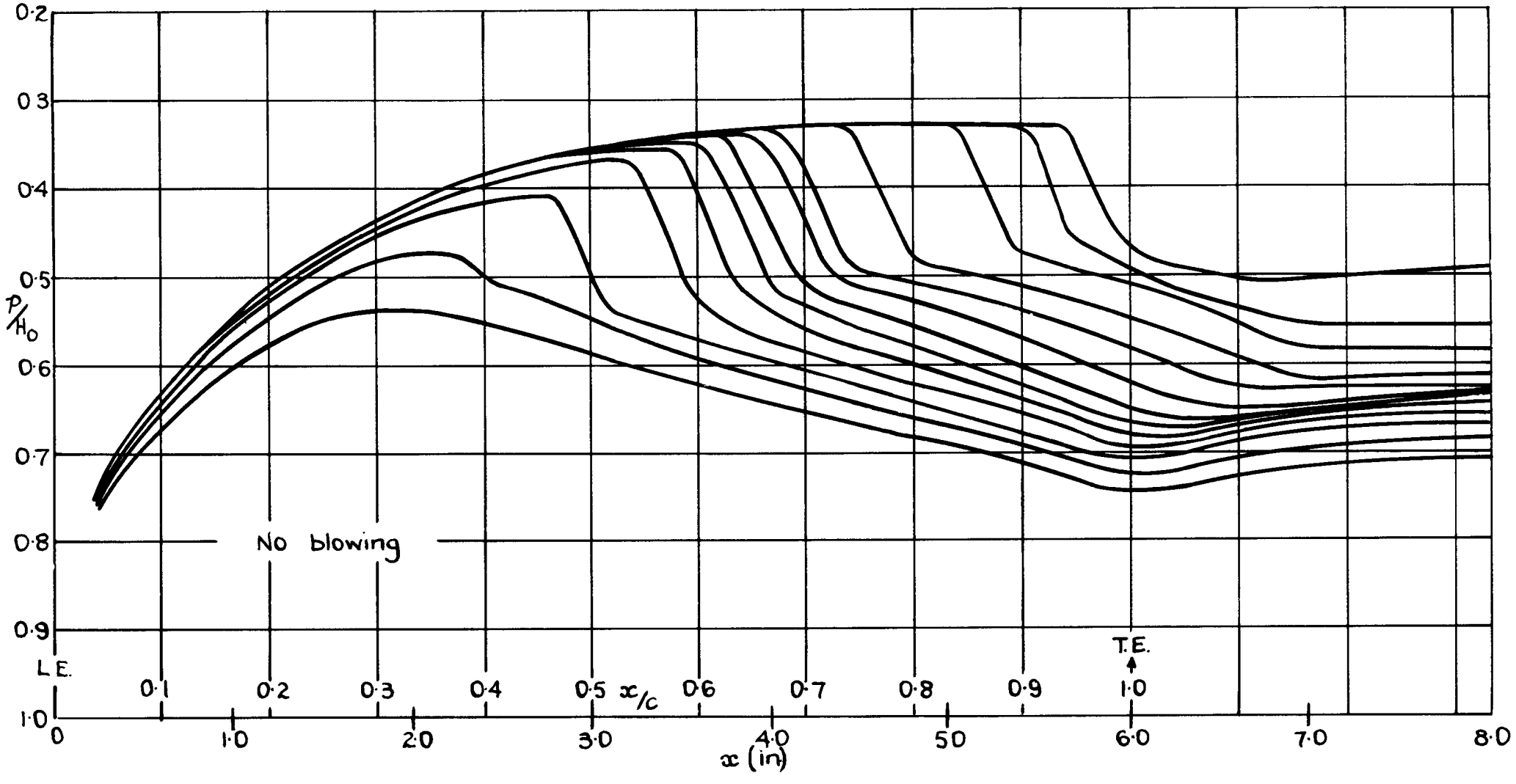

FIG 3

Distributions of static pressure along the 6% thick bump, No blowing.

FIG. 4.

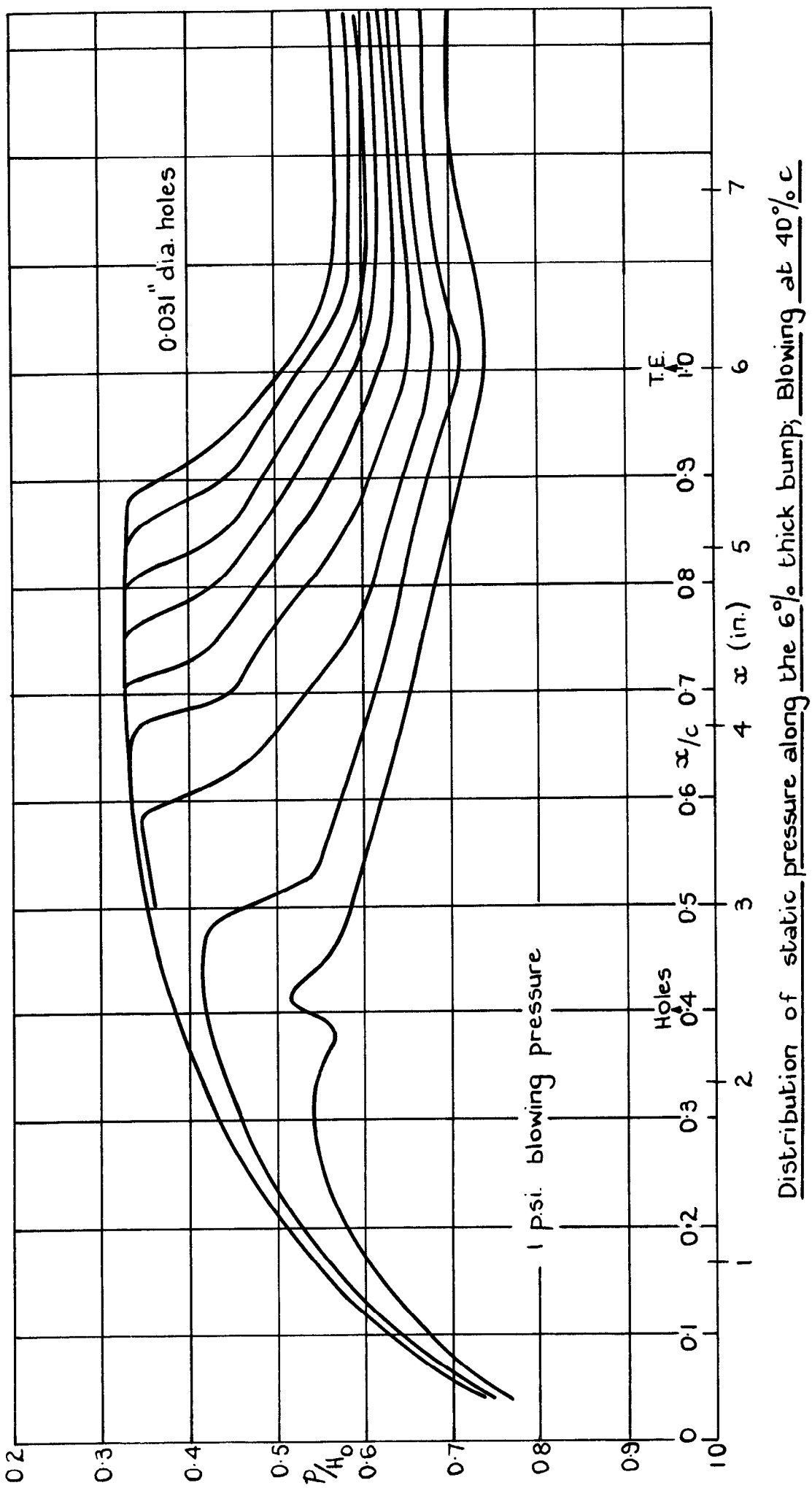

Distribution of static pressure along the 6% thick bump; Blowing at 40% c

FIG 5.

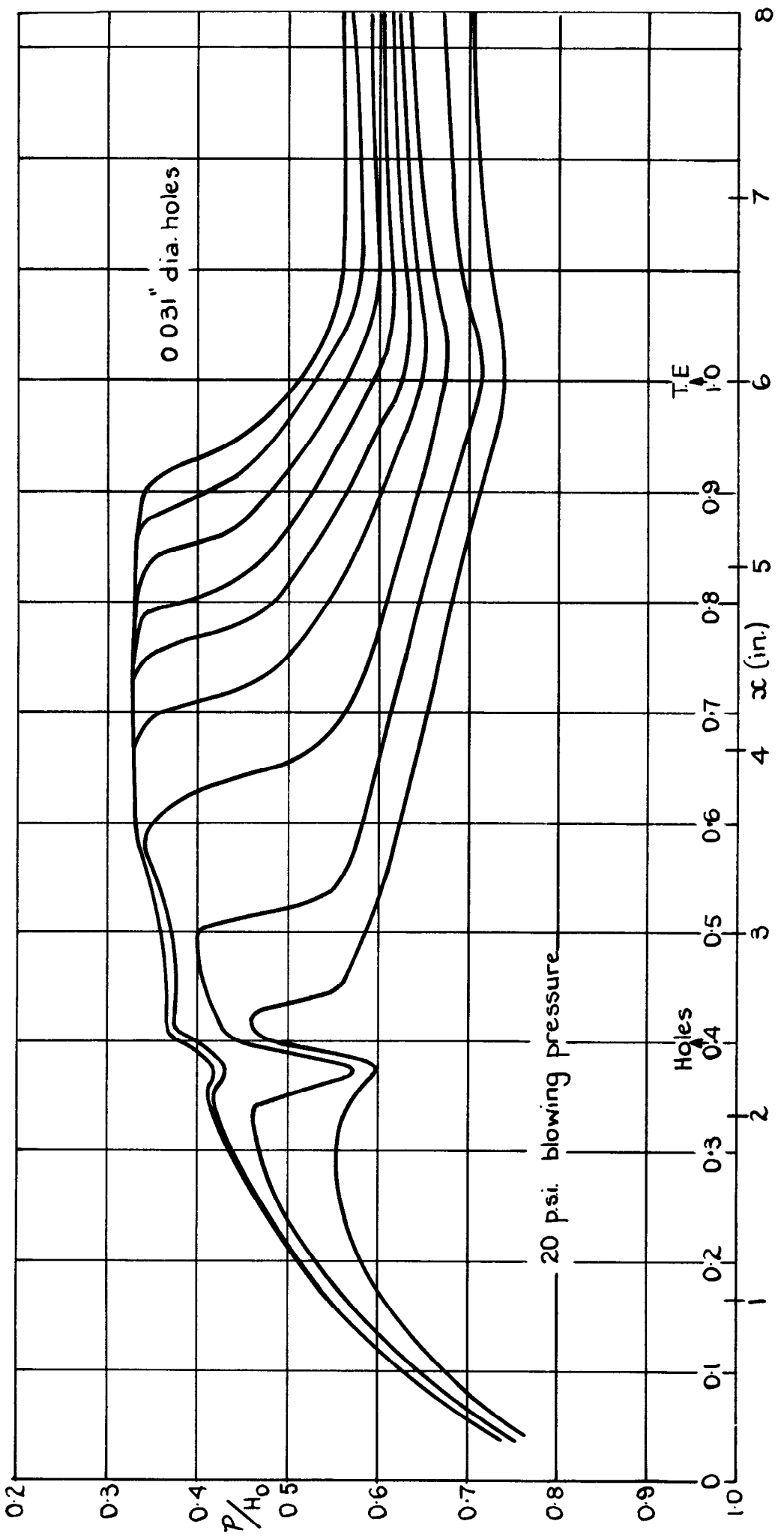

Distribution of static pressure along the 6% thick bump. Blowing at 40% c

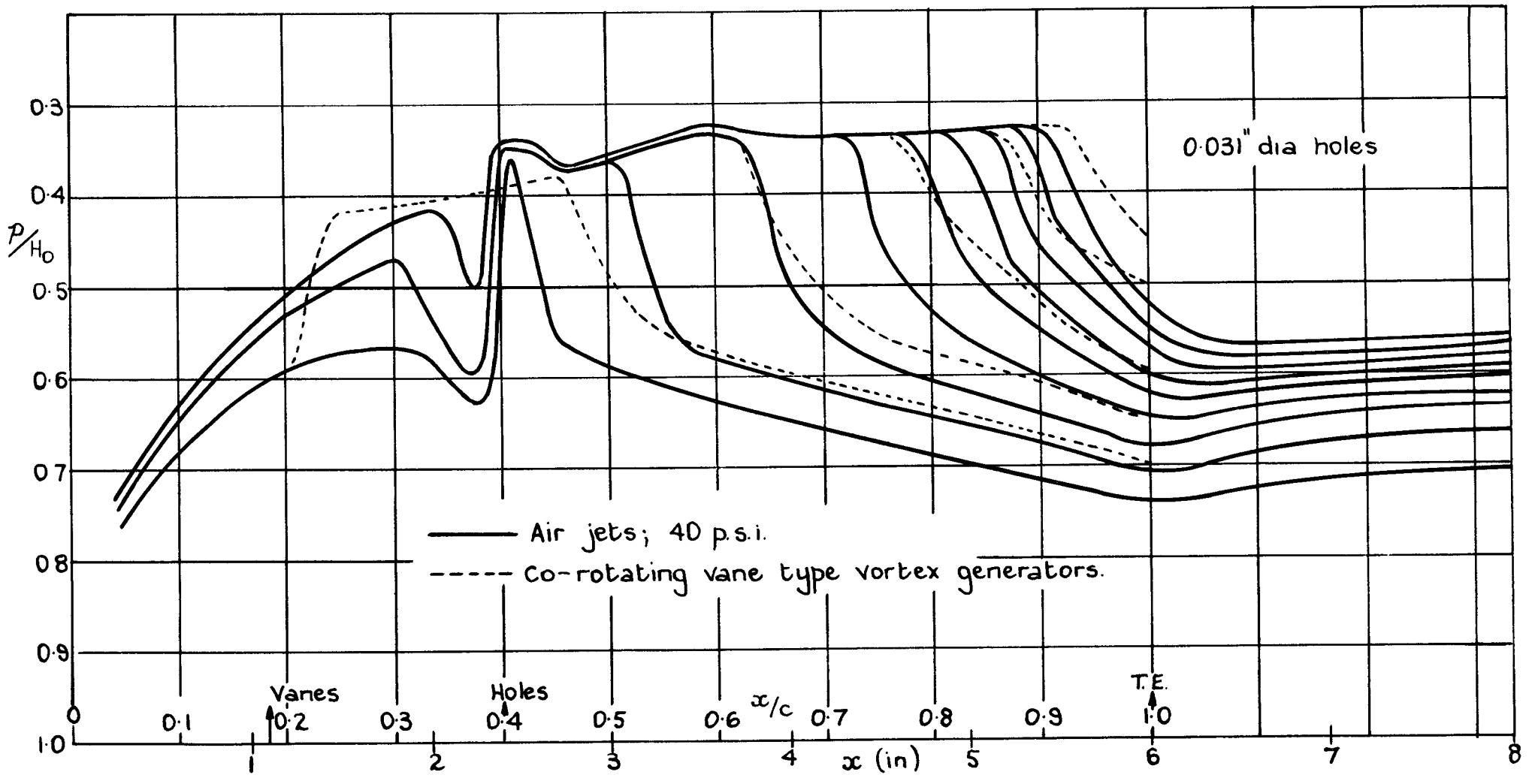

FIG 6.

Distribution of static pressure along the 6% thick bump; Blowing at 40% c
Comparison with vane type generators.

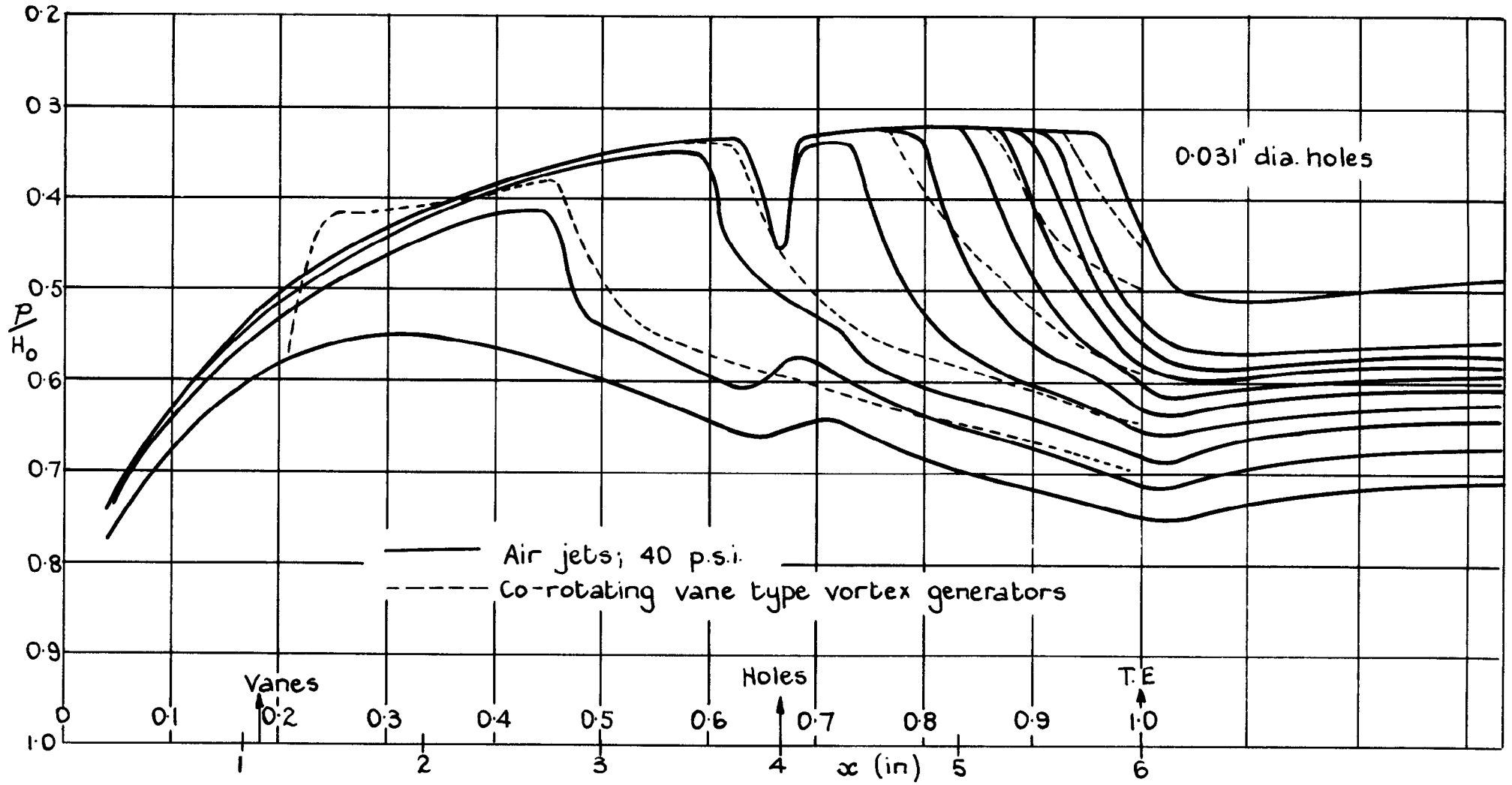

FIG. 7.

Distribution of static pressure along the 6% thick bump; Blowing at 66·7% c.
Comparison with vane type generators.

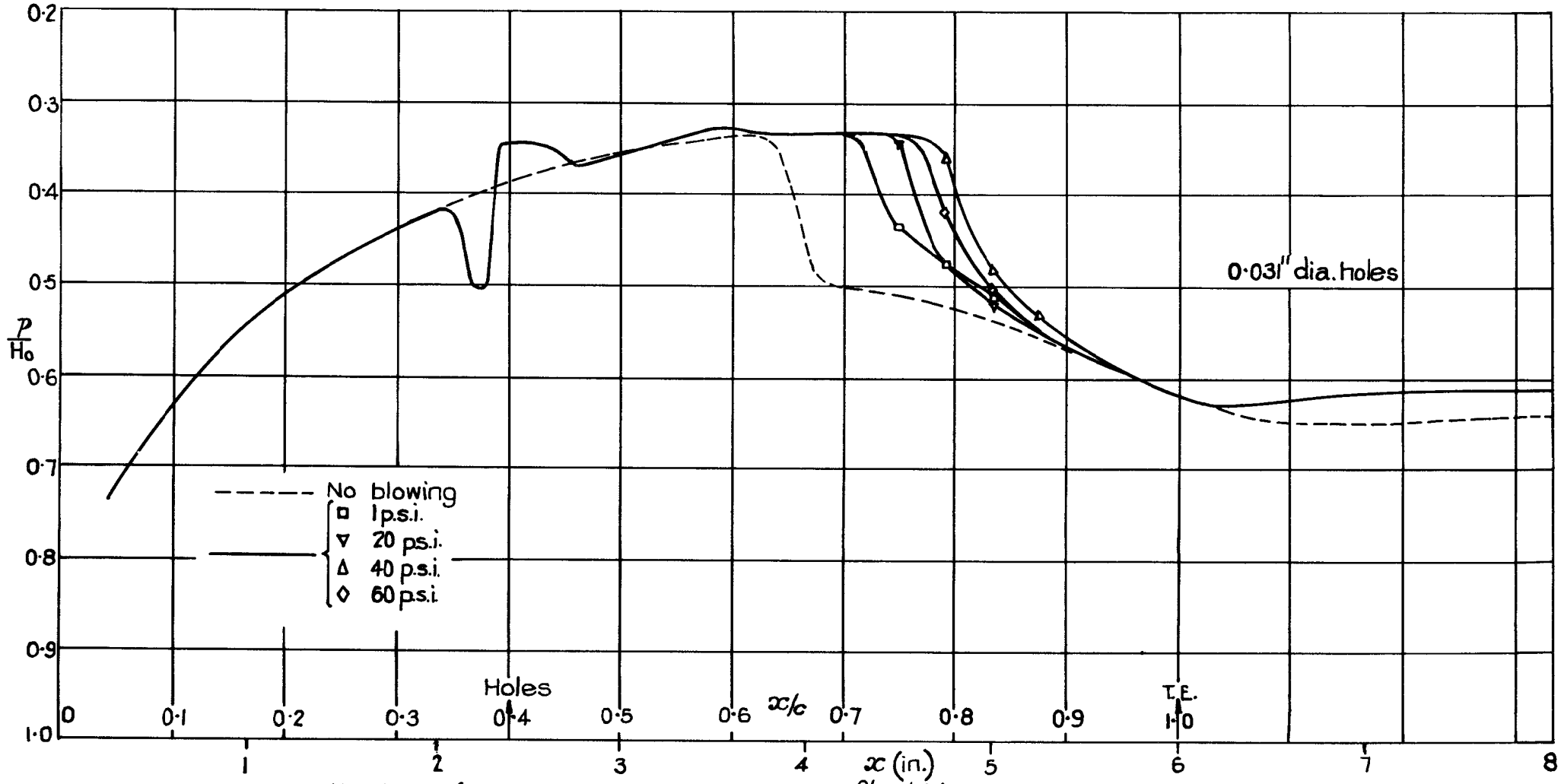

FIG. 8

Distribution of static pressure along the 6% thick bump. Blowing at 40% c
Effect of blowing pressure for constant trailing edge pressure $\left(\frac{p_{T.E.}}{H_0} = 0{\cdot}62\right)$

FIG. 9.

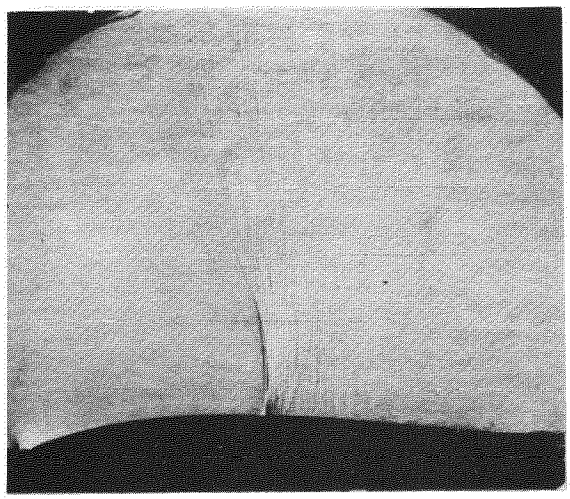

(a)

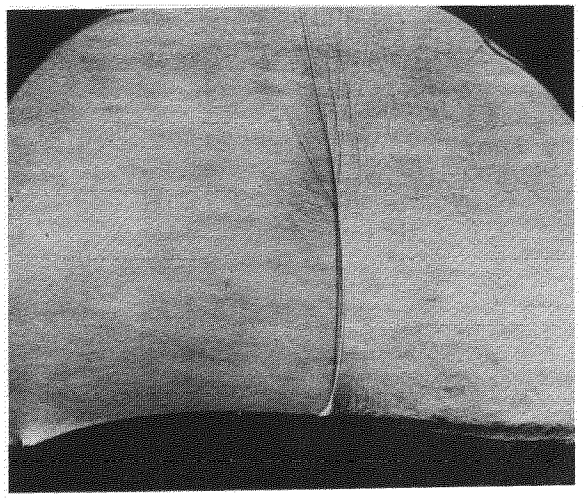

(b)

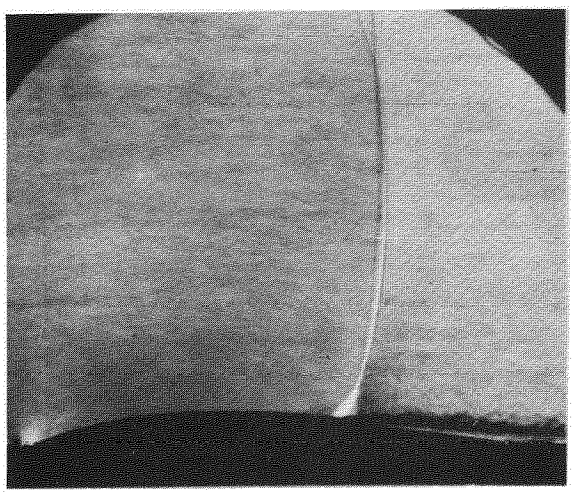

(c)

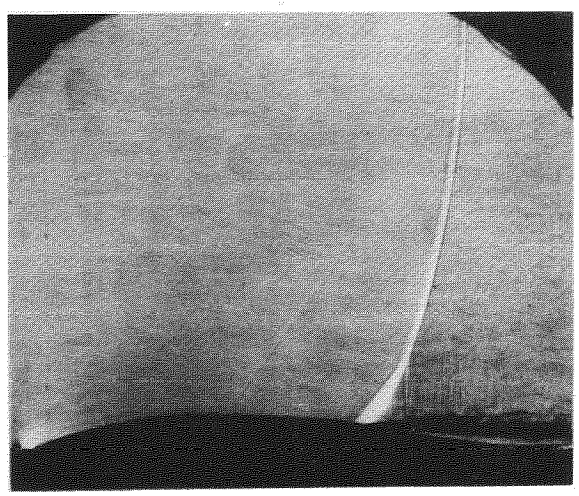

(d)

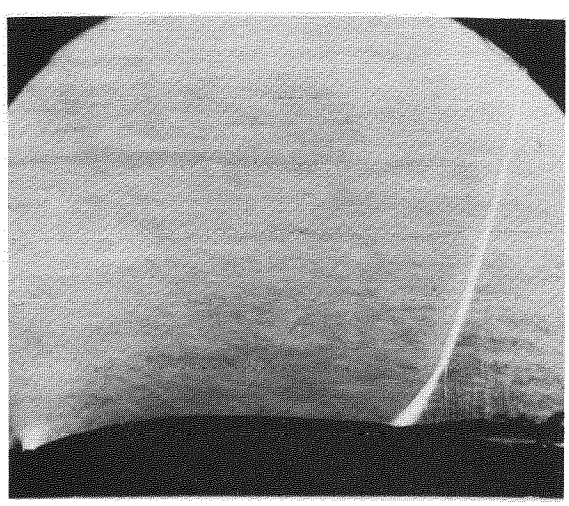

(e)

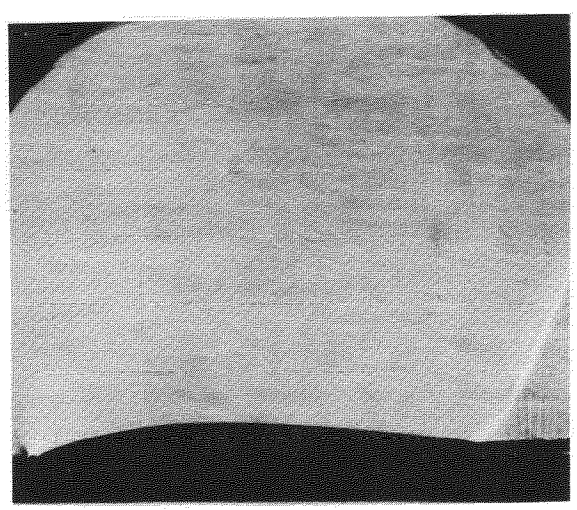

(f)

Schlieren photographs for the 6 % thick bump. No blowing.

FIG. 10.

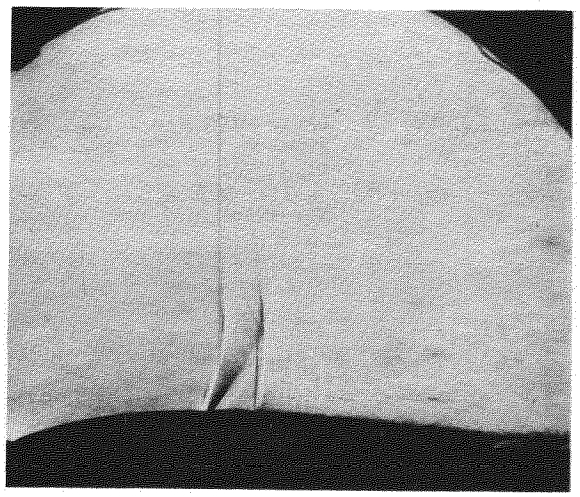

(a)

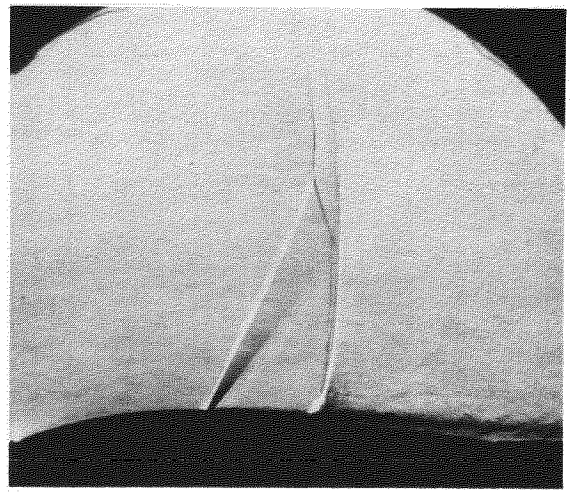

(b)

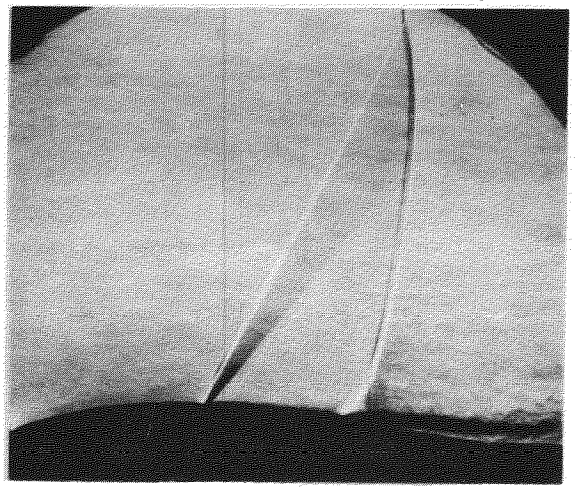

(c)

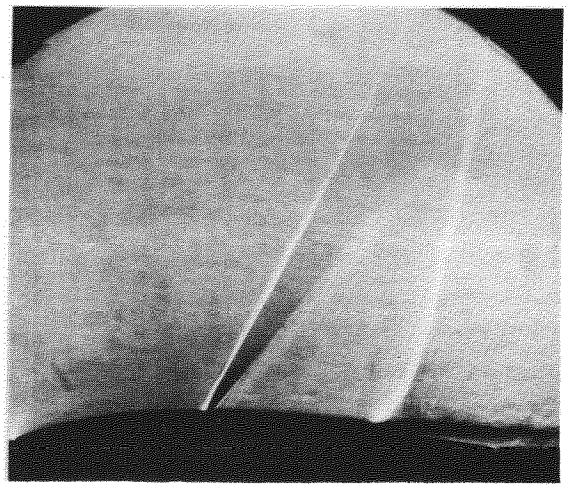

(d)

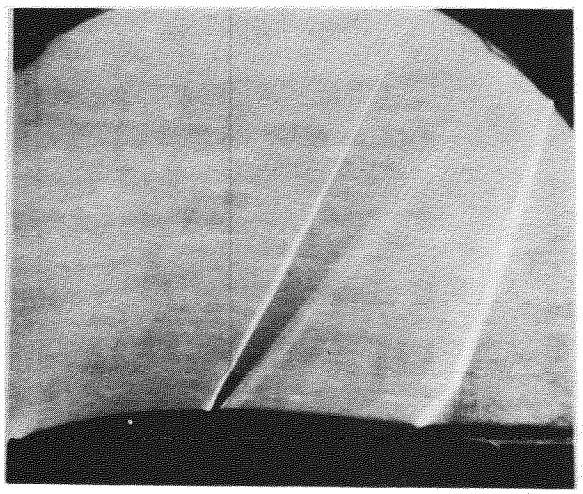

(e)

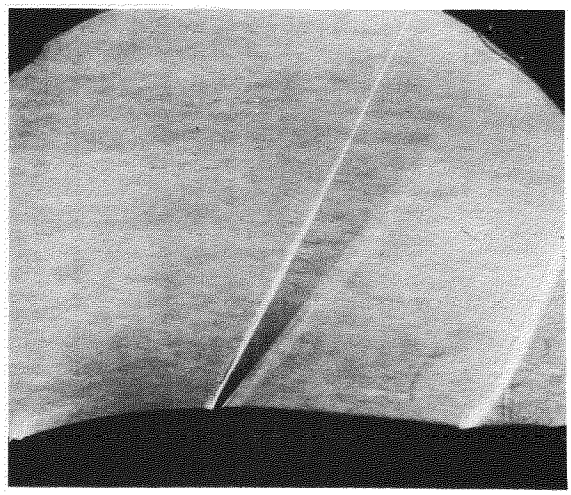

(f)

Schlieren photographs for the 6% thick bump. Plowing at 10°

FIG. 11.

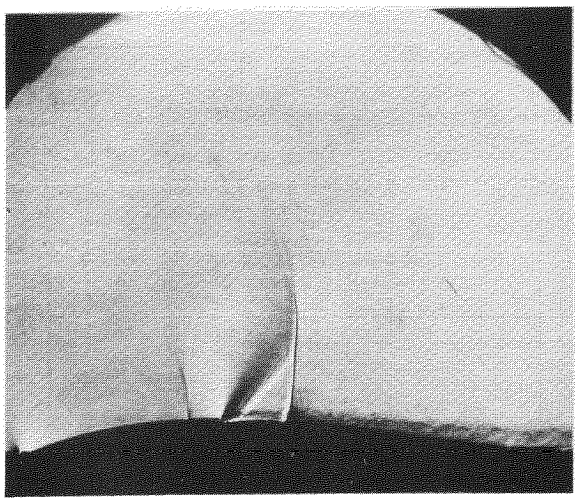

(a)

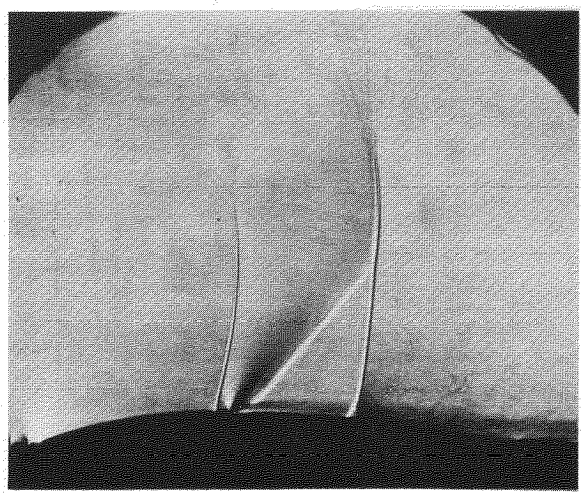

(b)

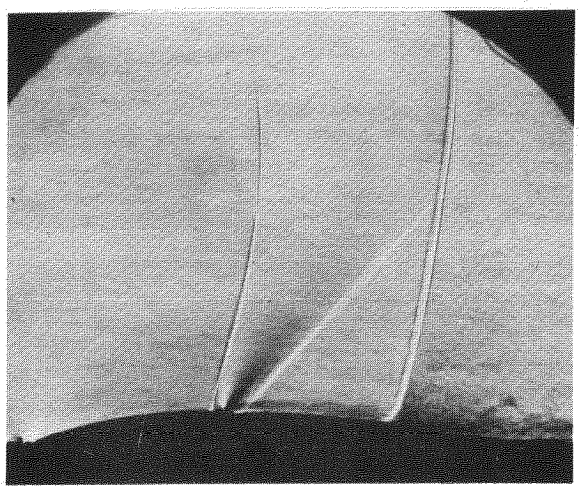

(c)

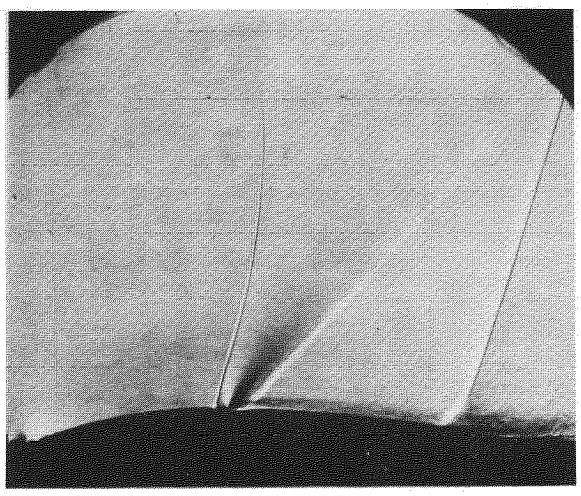

(d)

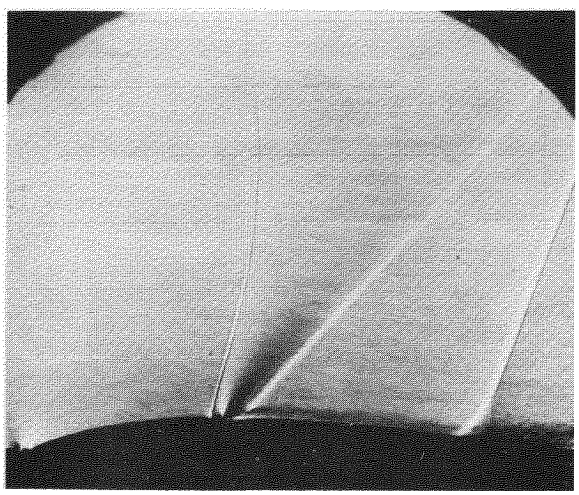

(e)

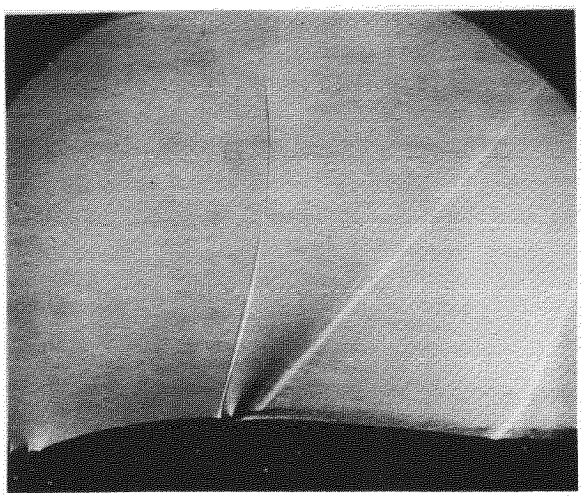

(f)

Schlieren photographs for the 6% thick bump. Blowing at 40% chord – 40 p.s.i.

FIG. 12.

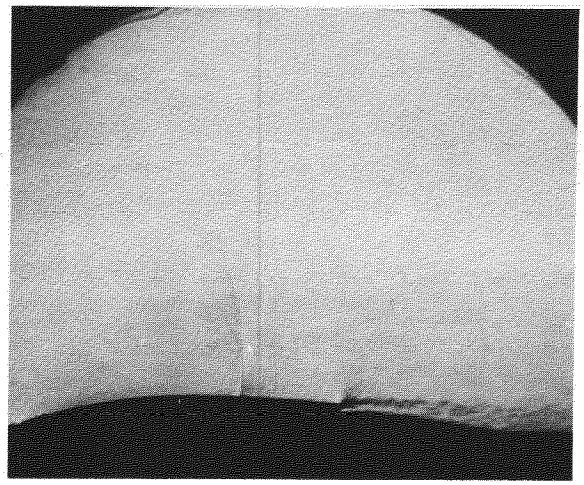

(a)

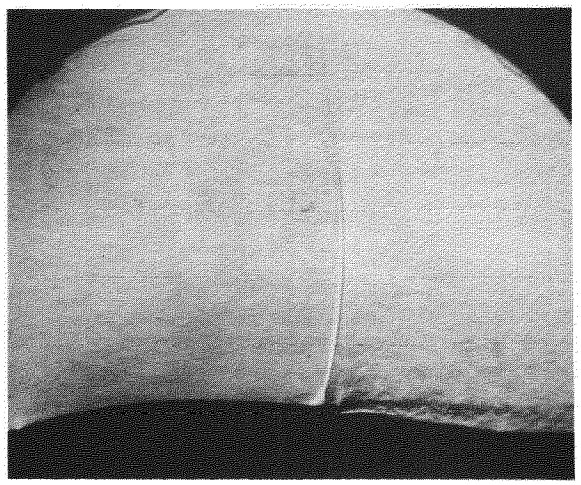

(b)

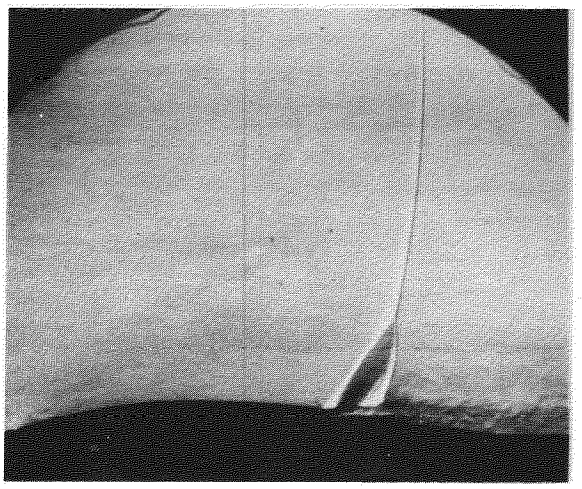

(c)

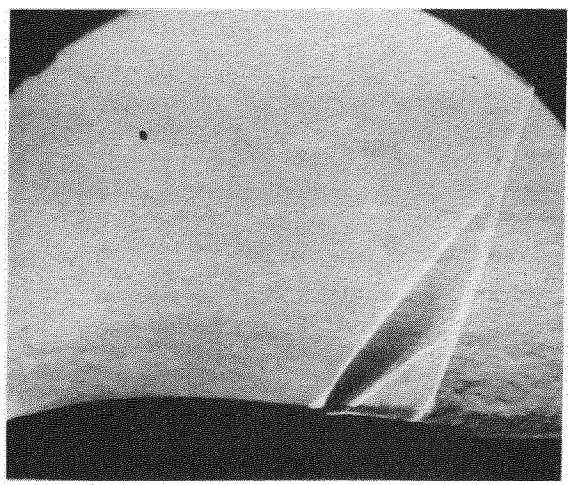

(d)

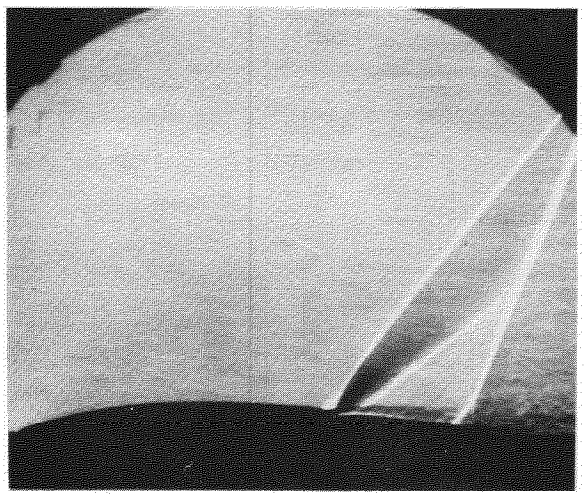

(e)

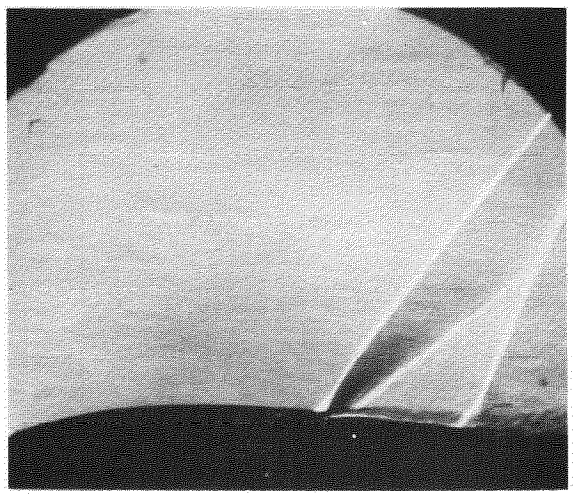

(f)

FIG. 13.

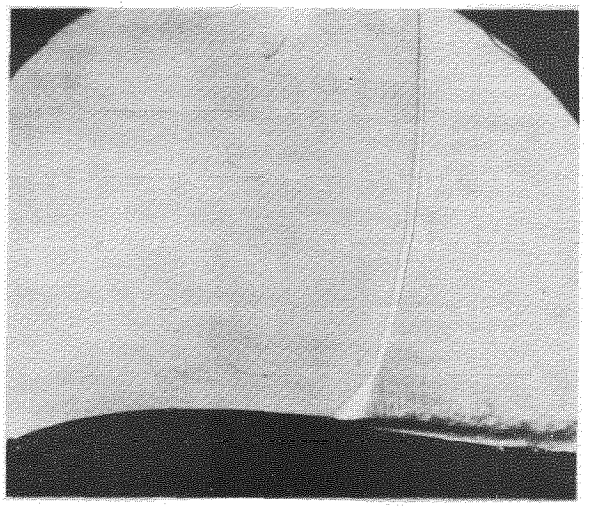

(a) No blowing

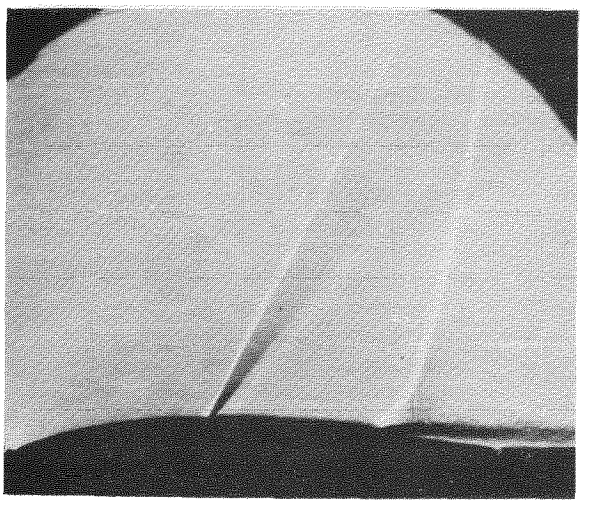

(b) 1 p.s.i.

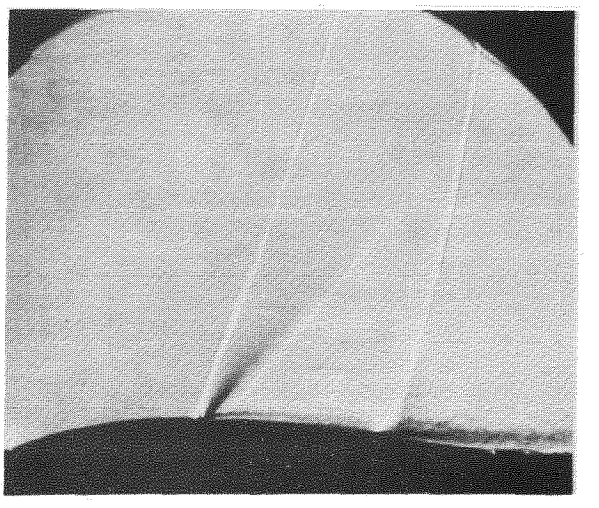

(c) 20 p.s.i.

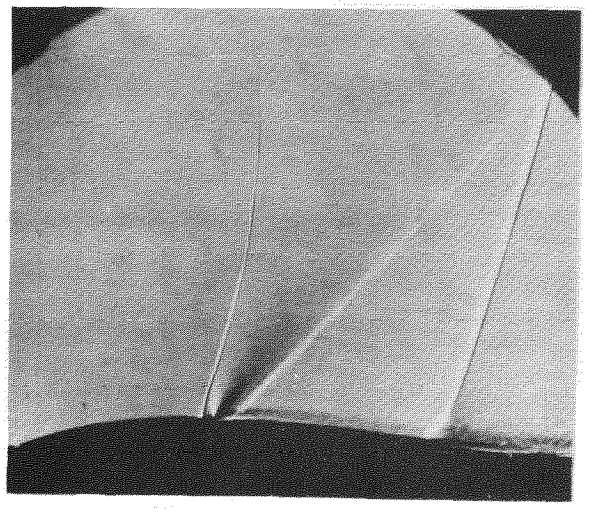

(d) 40 p.s.i.

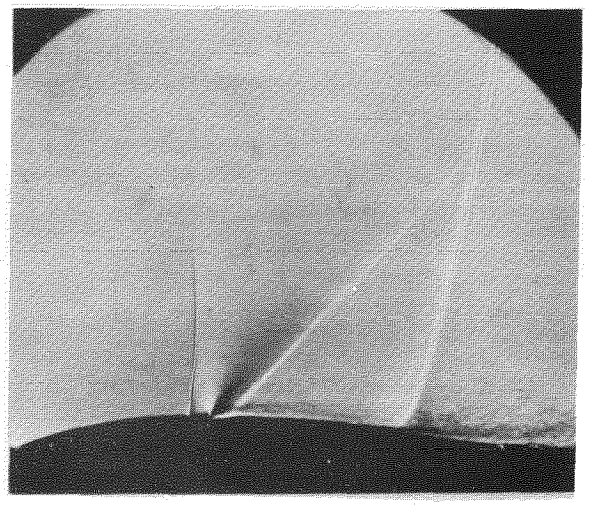

(e) 60 p.s.i.

Schlieren photographs for the 6% thick bump. Blowing at 40% chord.

FIG. 14.

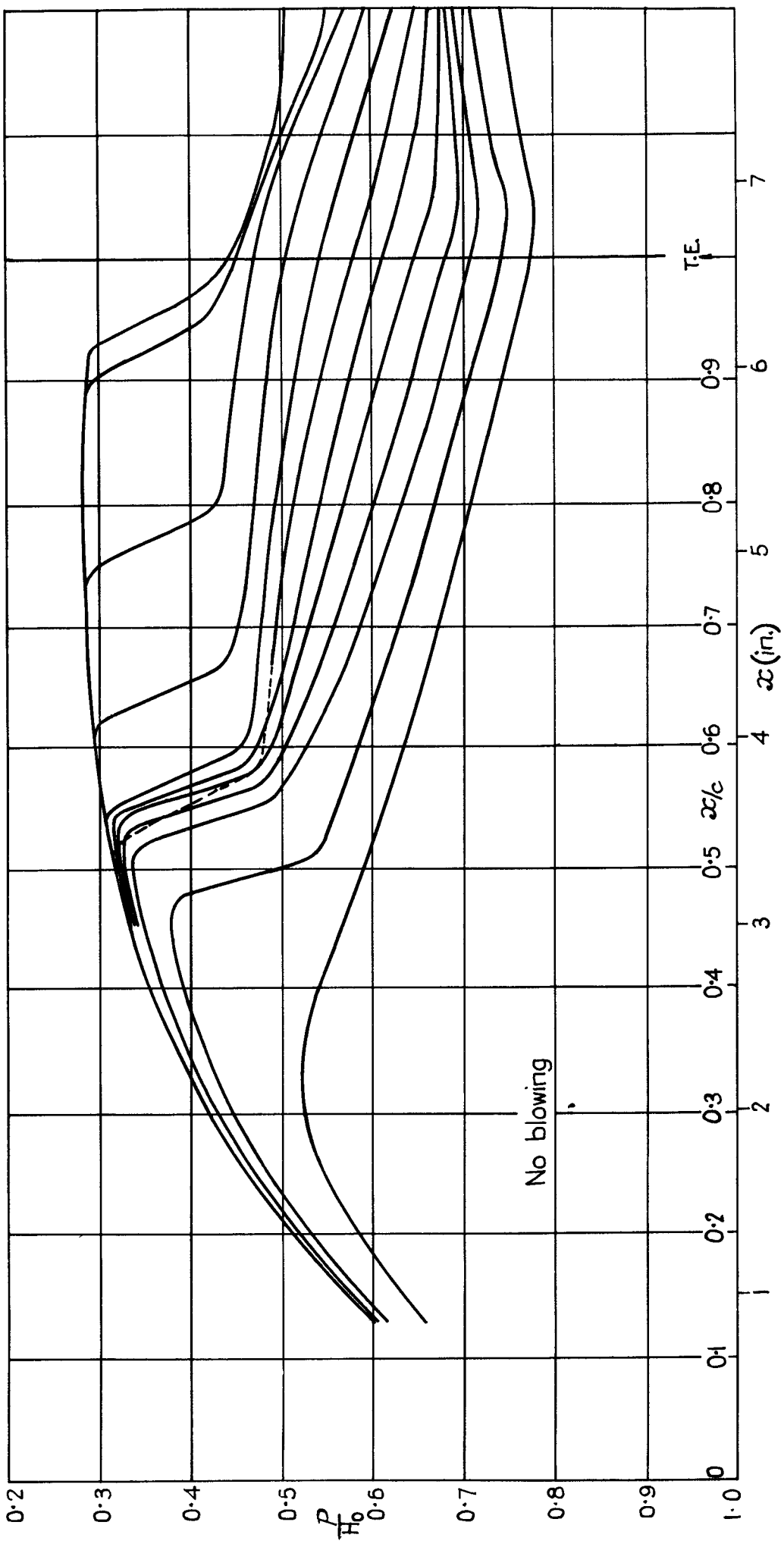

Distribution of static pressure along the 8% thick bump.

FIG. 15.

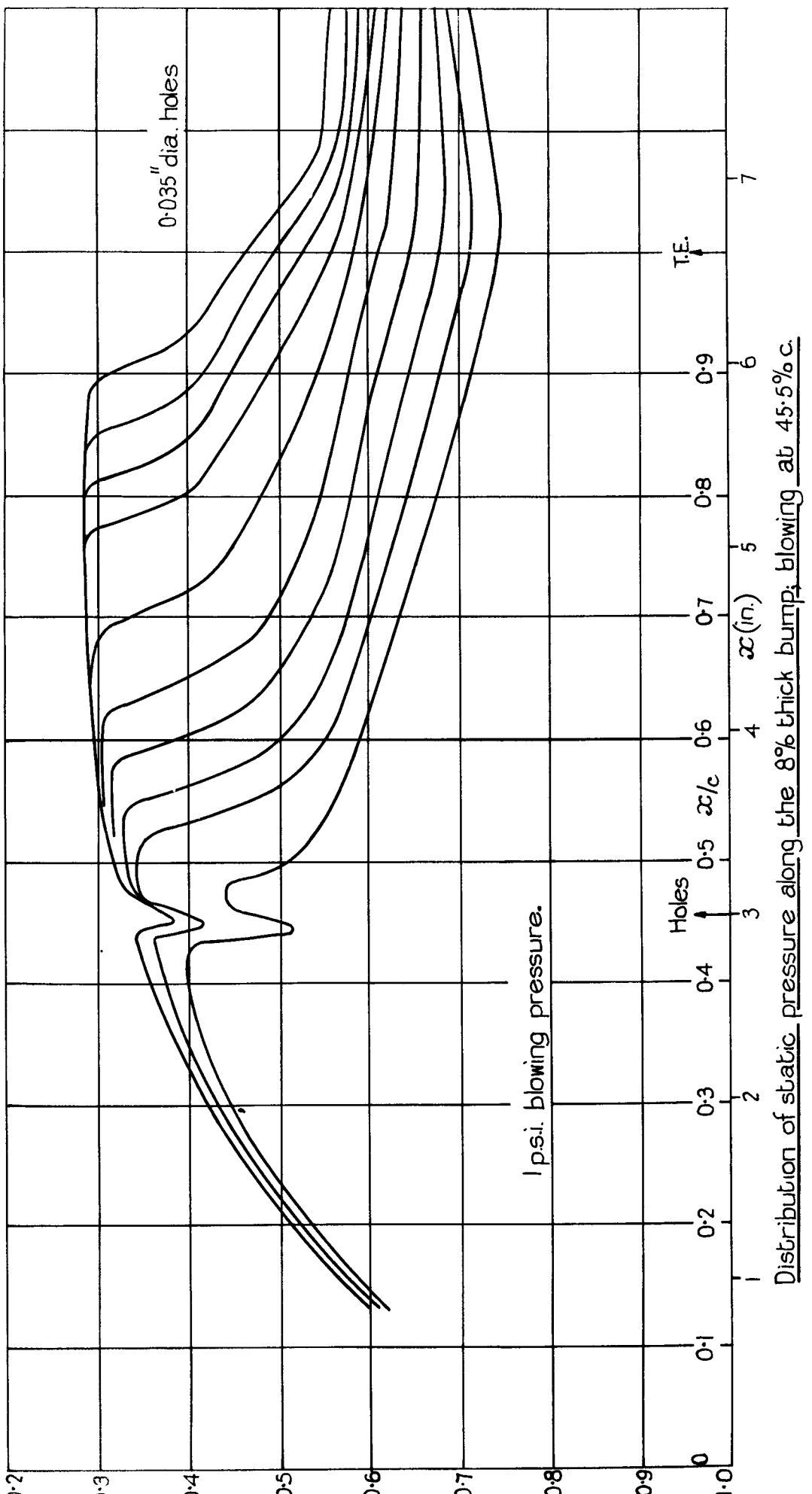

Distribution of static pressure along the 8% thick bump, blowing at 45·5% c.

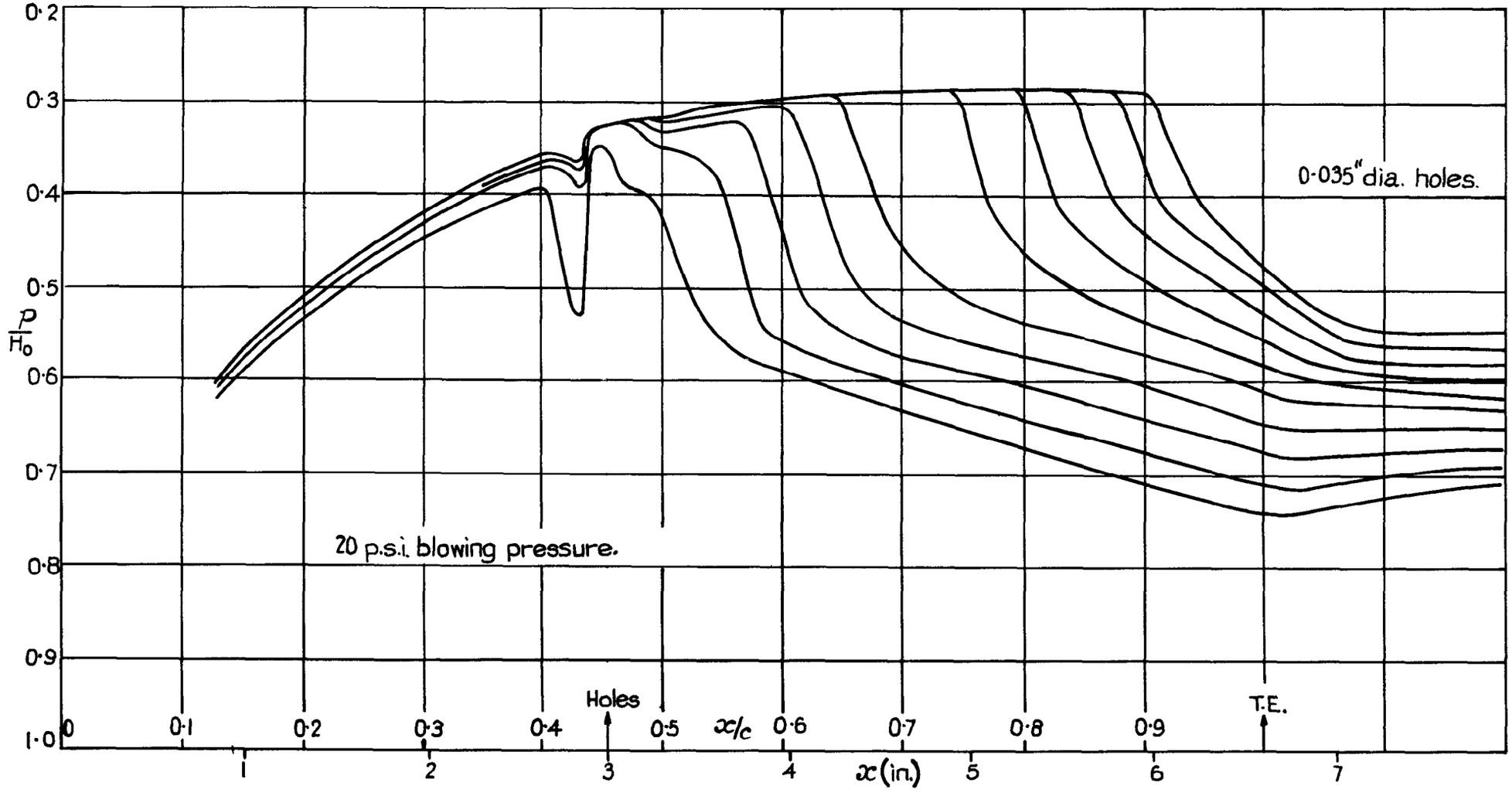

Distribution of static pressure along 8% thick bump; blowing at 45·5% c.

FIG. 16.

FIG. 17.

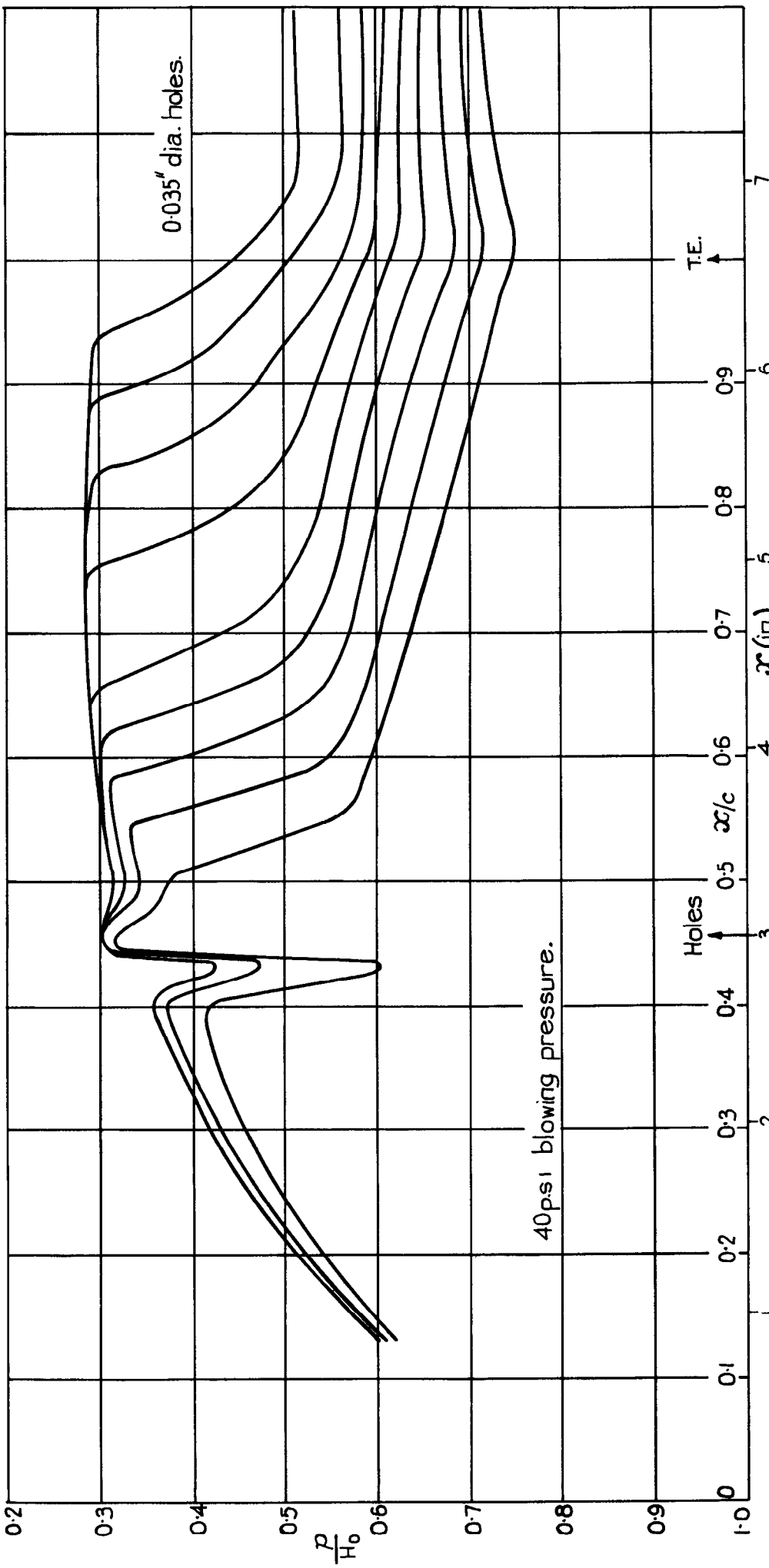

Distribution of static pressure along the 8% thick bump, blowing at 45·5% c

FIG. 18.

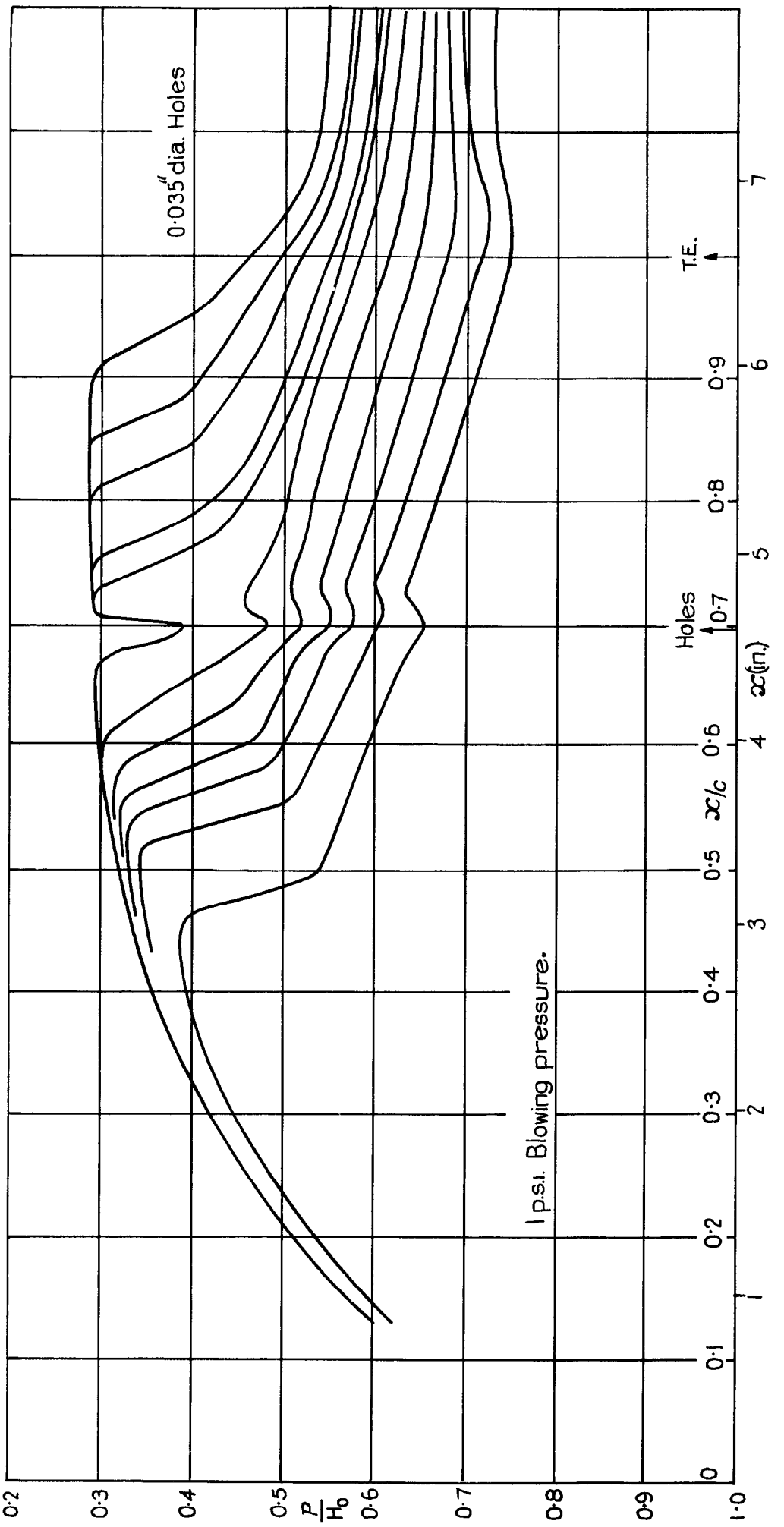

Distribution of static pressure along the 8% thick bump: blowing at 69·7% c

FIG. 19

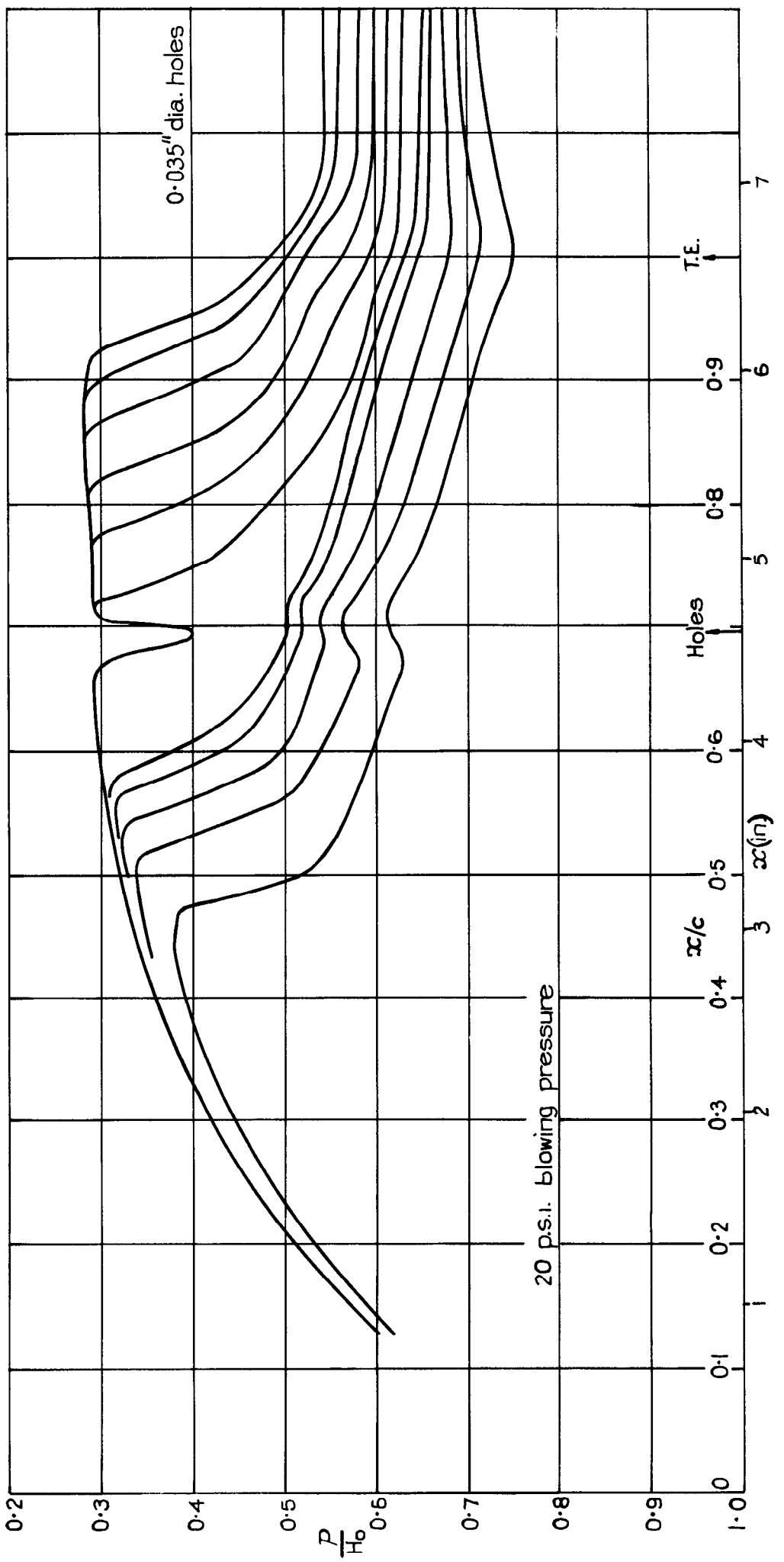

Distribution of static pressure along the 8% thick bump. Blowing at 69·7% c.

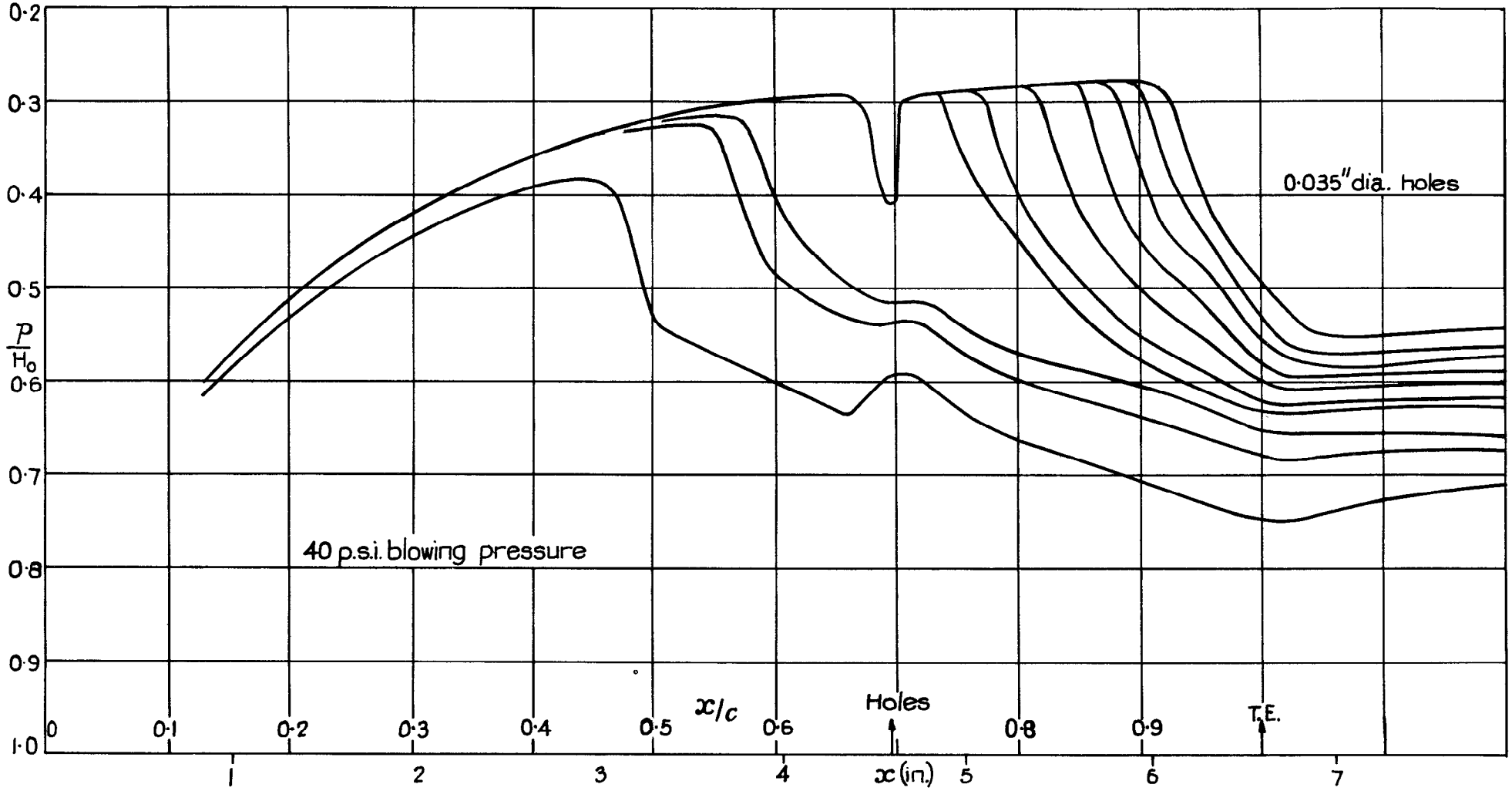

Distribution of static pressure along the 8% thick bump. Blowing at 69·7% c.

FIG. 20.

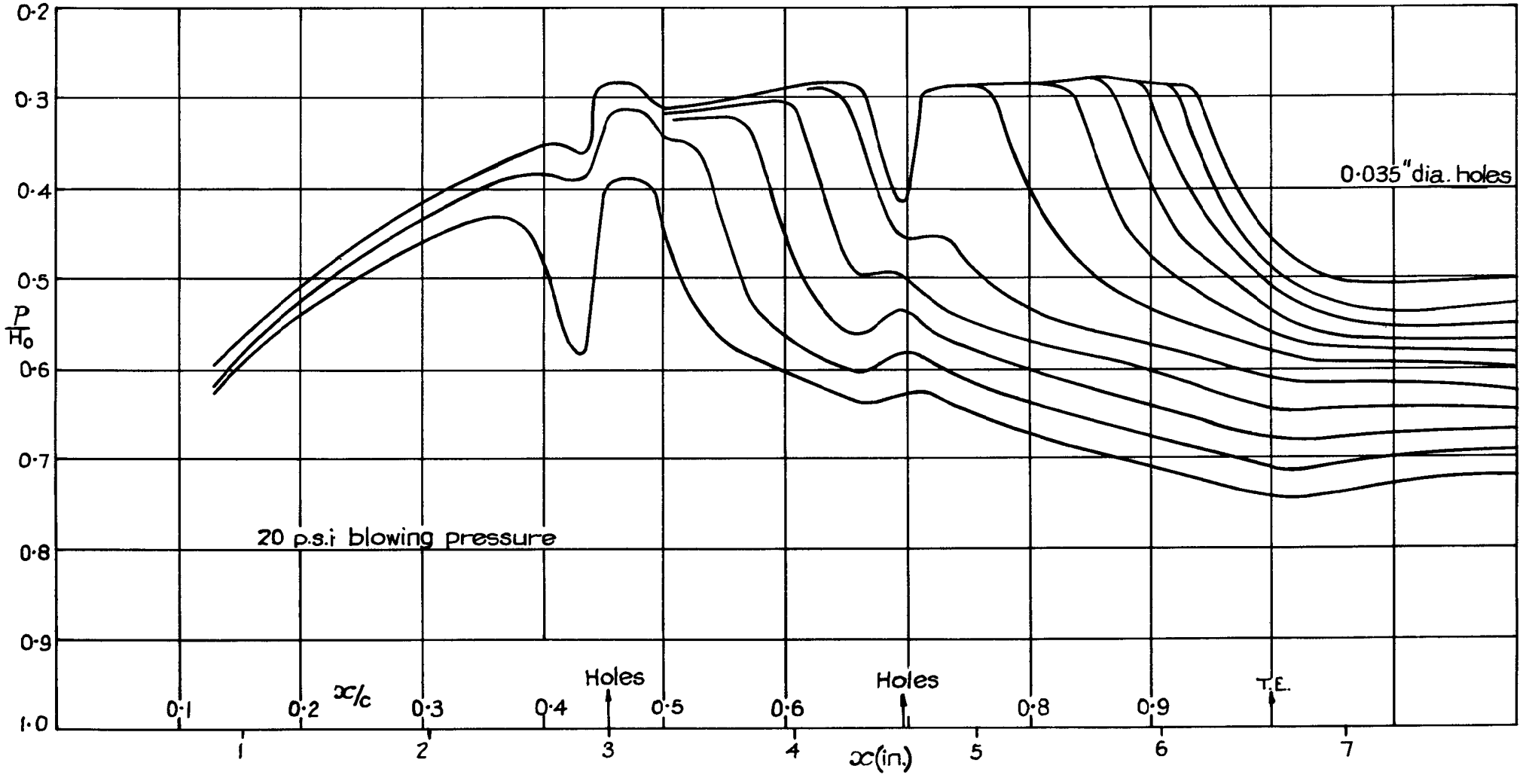

Variation of static pressure along the 8% thick bump. Blowing at 45·5% c and 69·7 %c

FIG. 21.

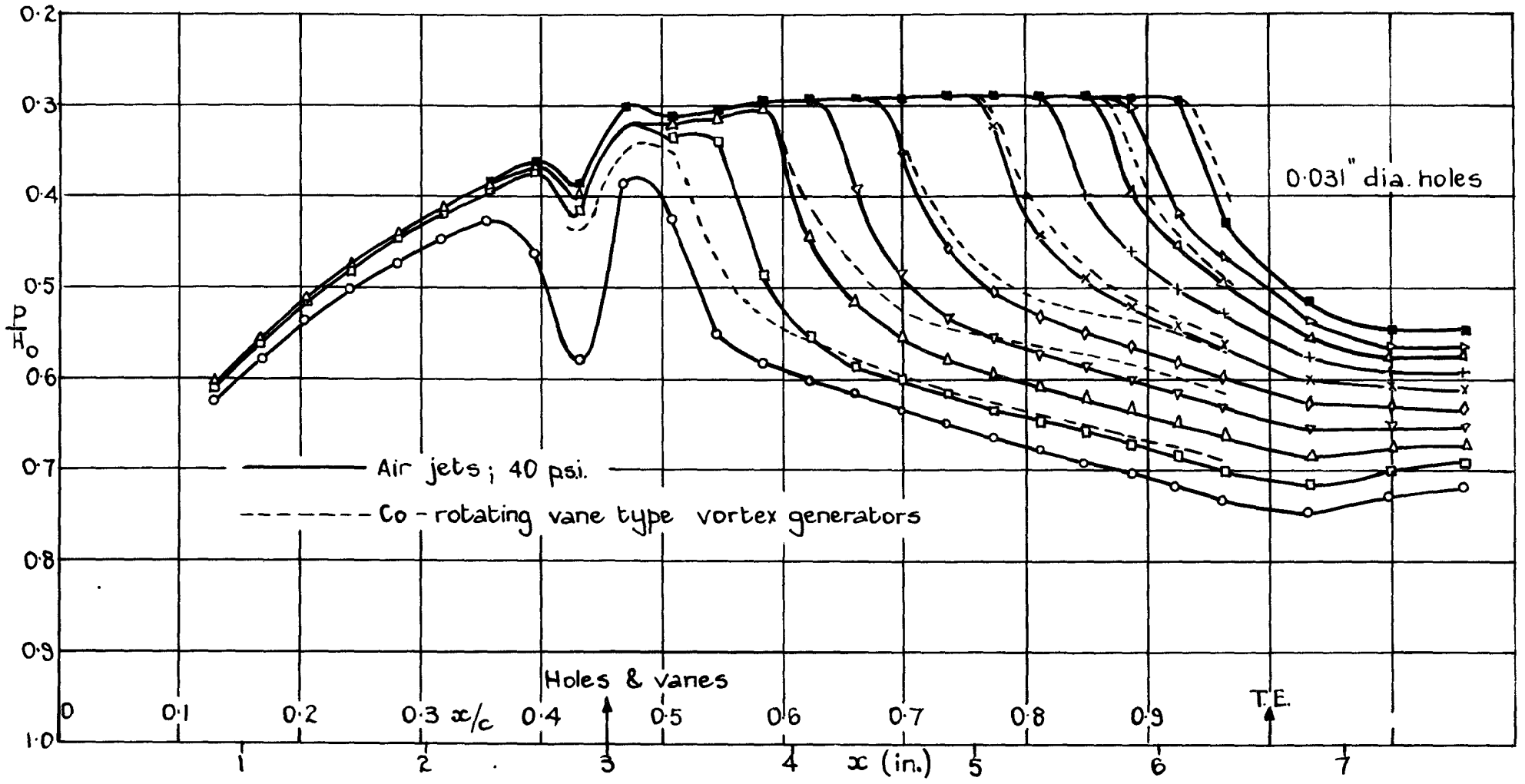

FIG. 22

Distributions of static pressure along the 8% thick bump: Blowing at 45·5% c
Comparison with vane-type vortex generators.

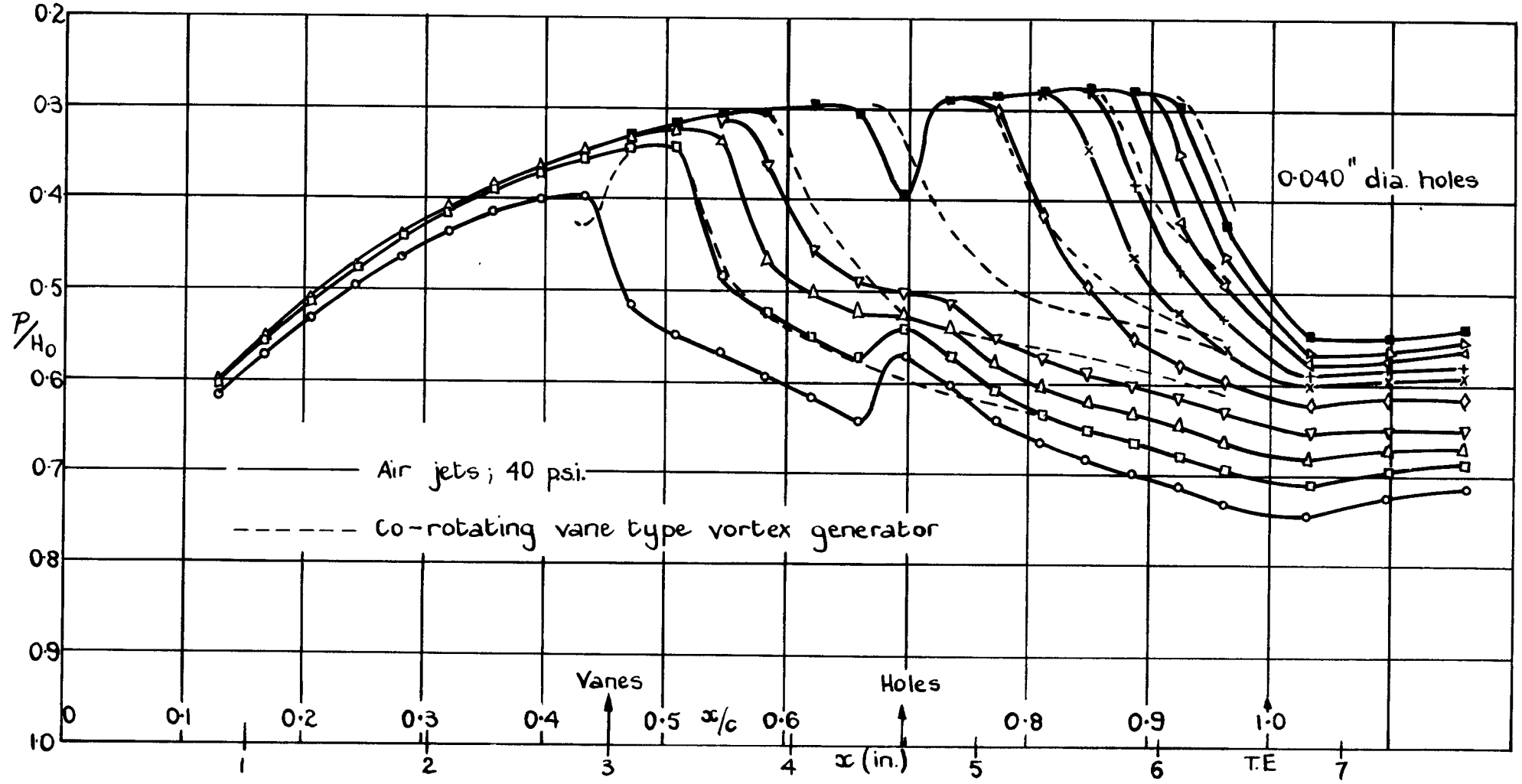

Distributions of static pressure along the 8% thick bump; Blowing at 69 7% c
Comparison with vane-type vortex generators.

FIG 23

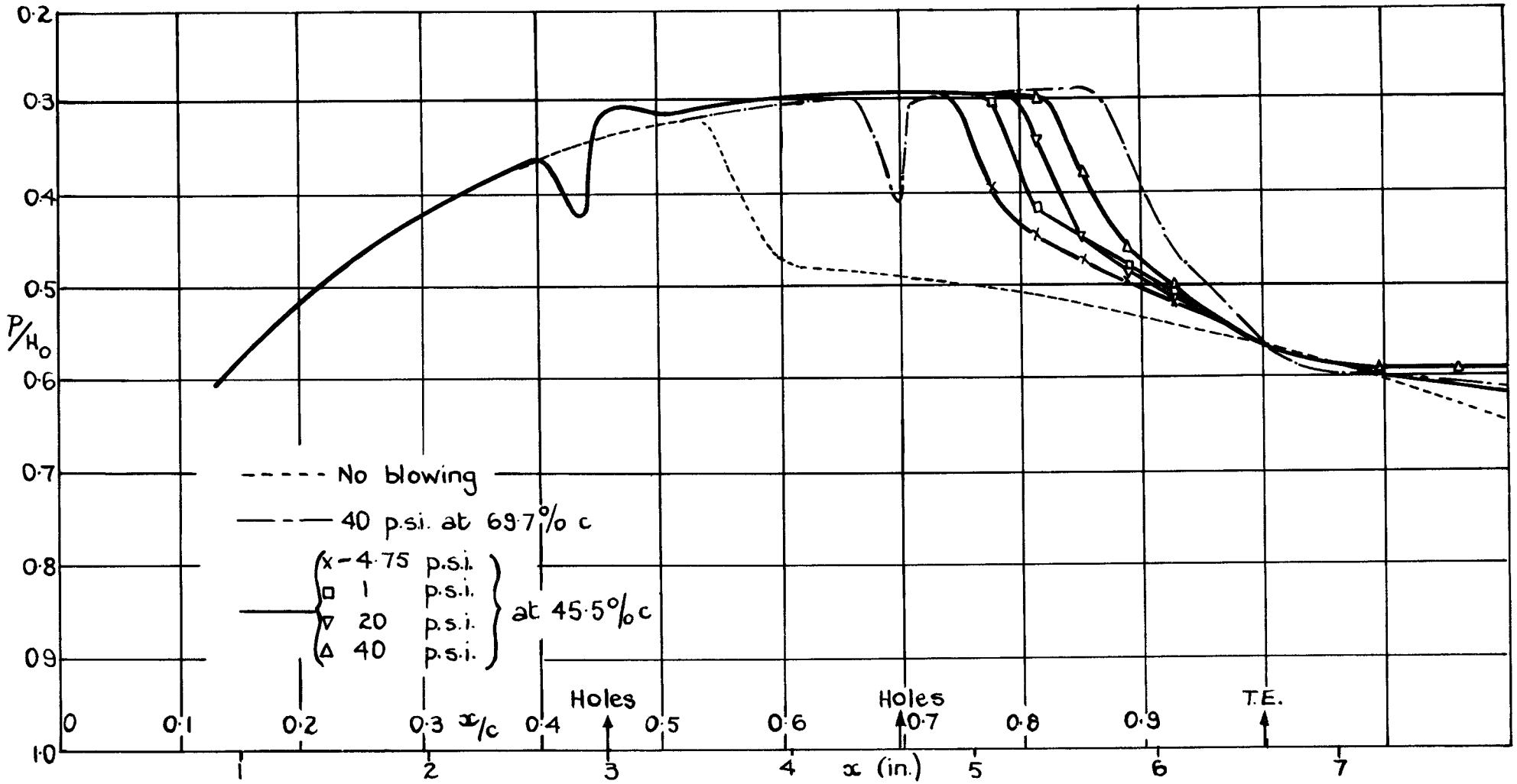

Distribution of static pressure along the 8% thick bump. Effect of blowing pressure for constant T.E pressure ($P/H_0 = 0.56$)

FIG. 24

FIG. 25.

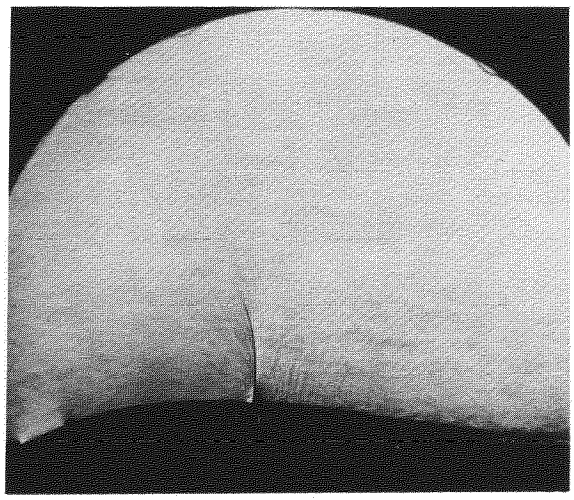

(a)

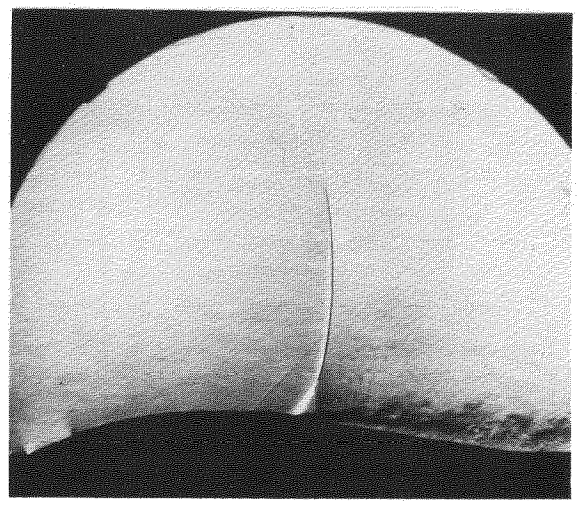

(b)

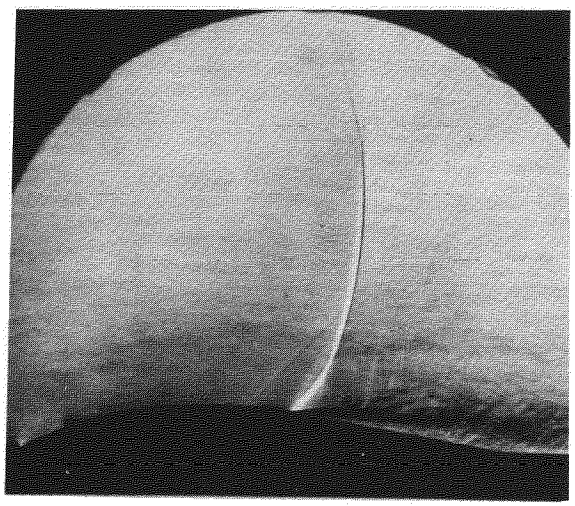

(c)

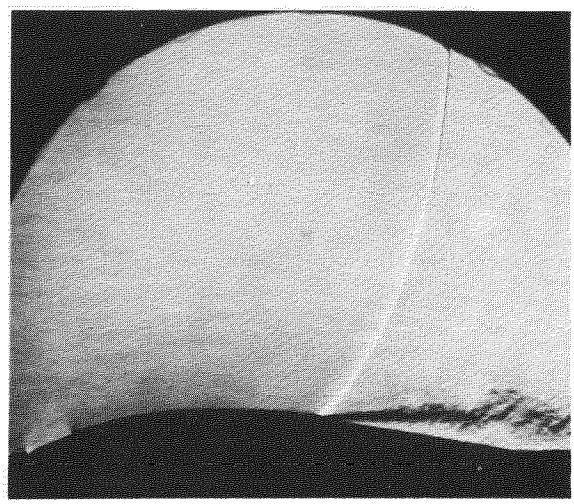

(d)

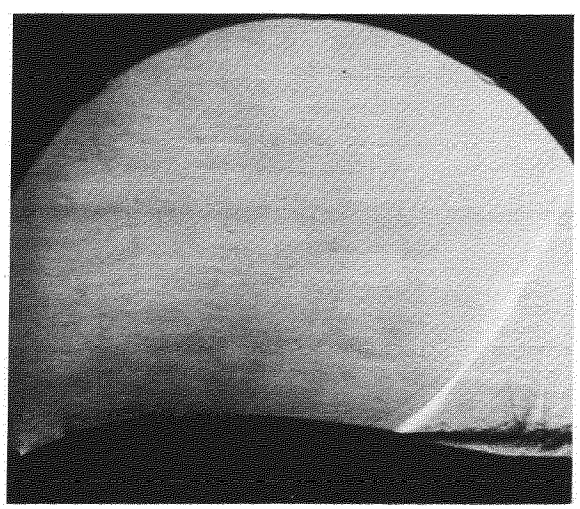

(e)

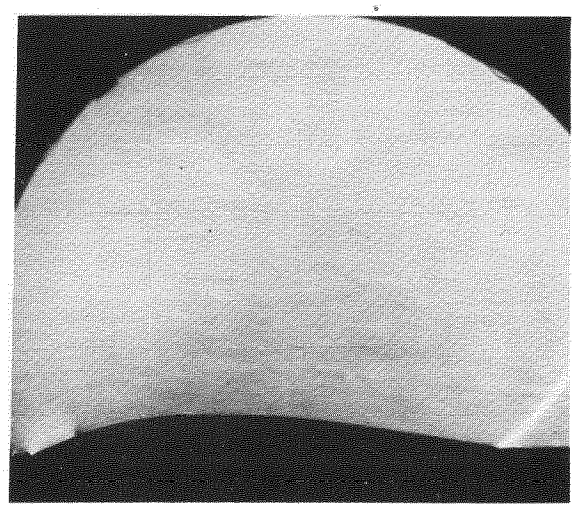

(f)

Schlieren photographs for the 8% thick bump. No blowing.

FIG.26.

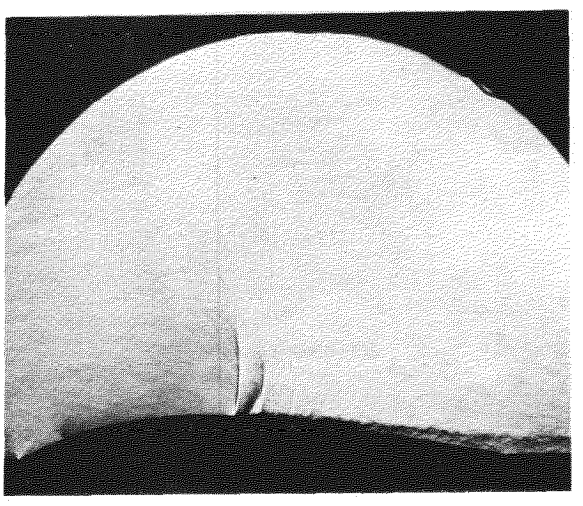

(a)

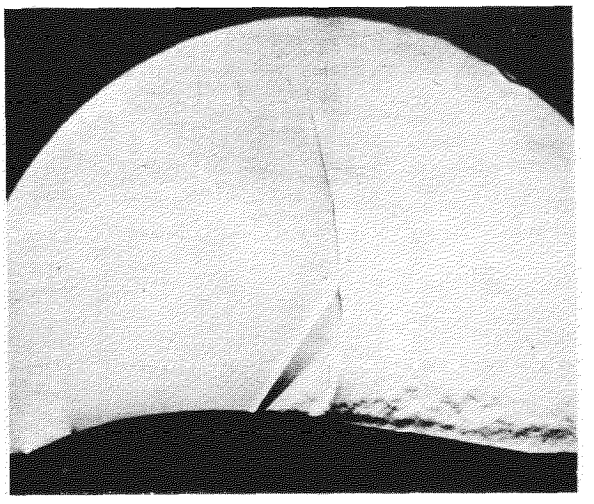

(b)

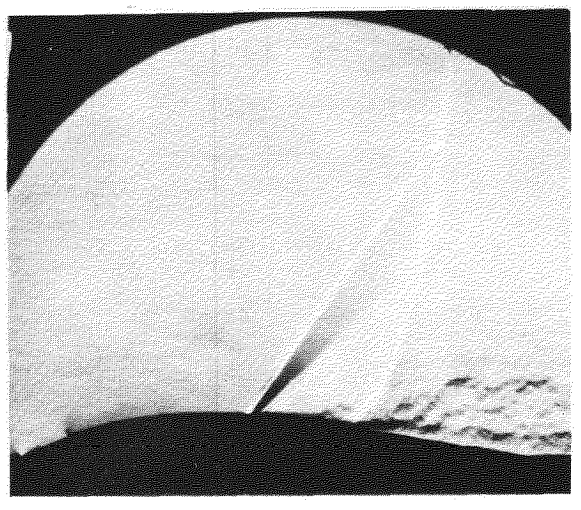

(c)

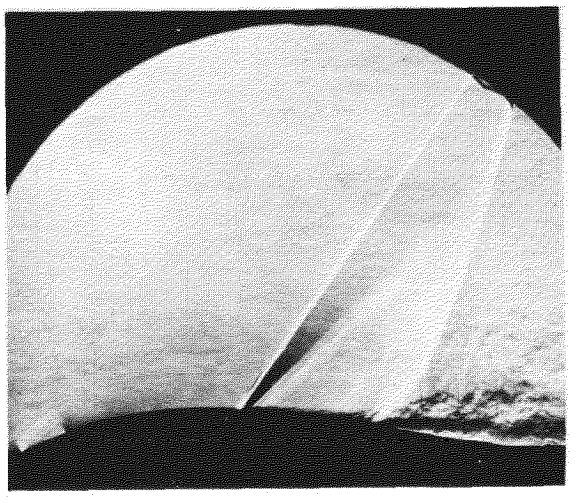

(d)

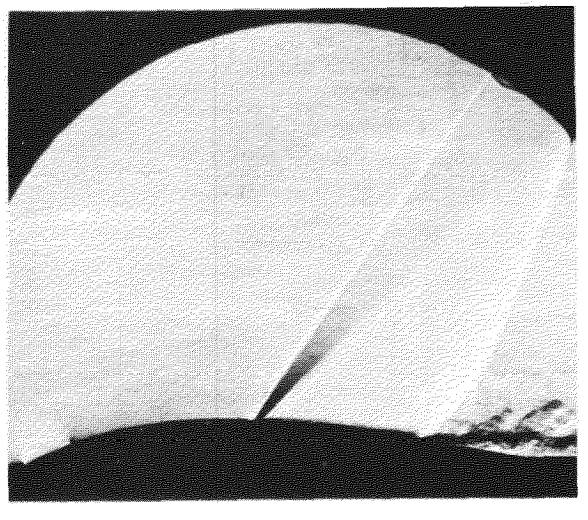

(e)

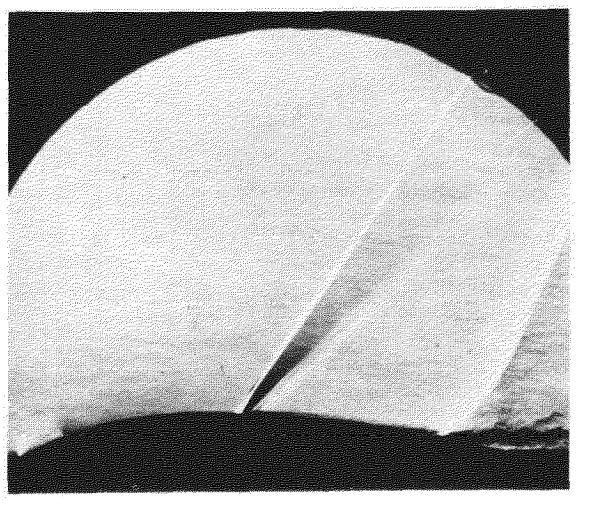

(f)

Schlieren photographs for the 8% thick bump. Blowing at 45·5% chord—1 p.s.i.

FIG. 27.

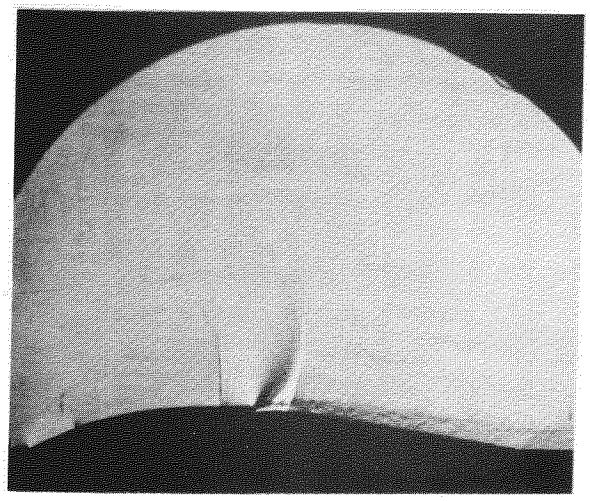

(a)

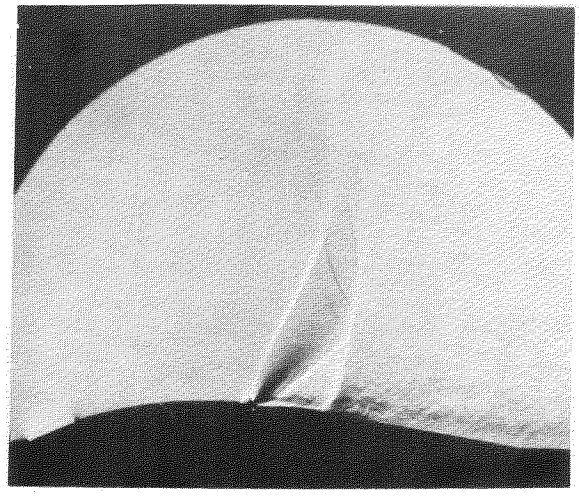

(b)

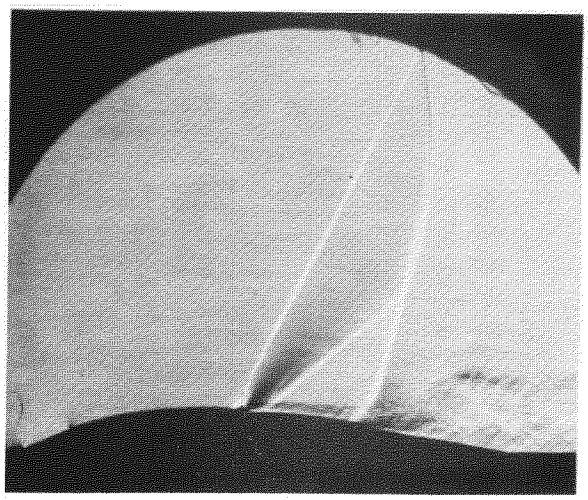

(c)

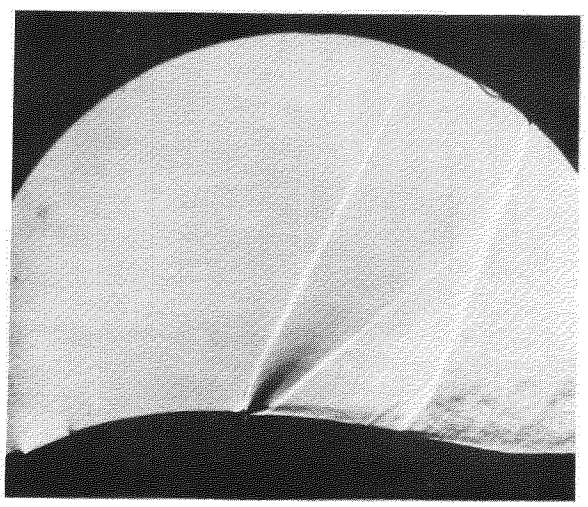

(d)

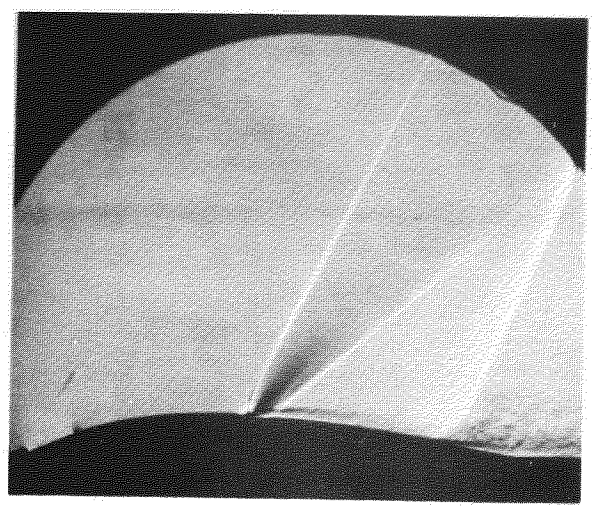

(e)

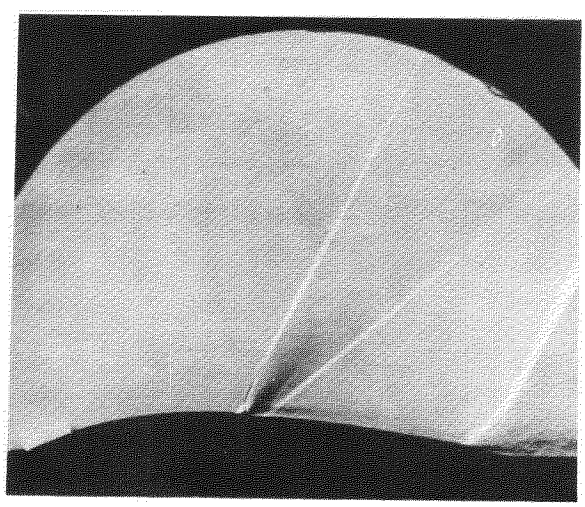

(f)

Schlieren photographs for the 8% thick bump. Blowing at 45·5% chord—40 p.s.i.

FIG. 28.

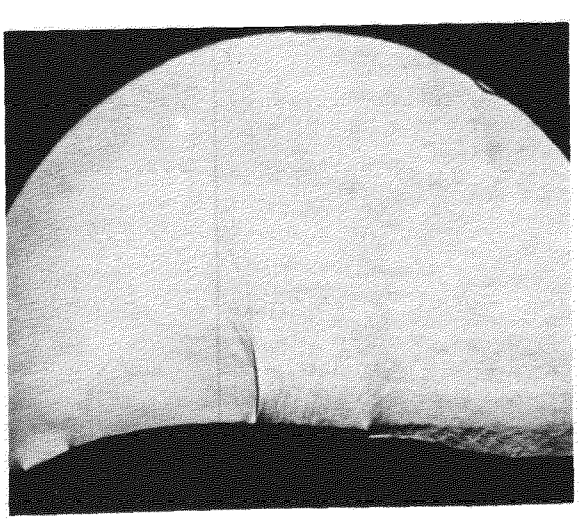

(a)

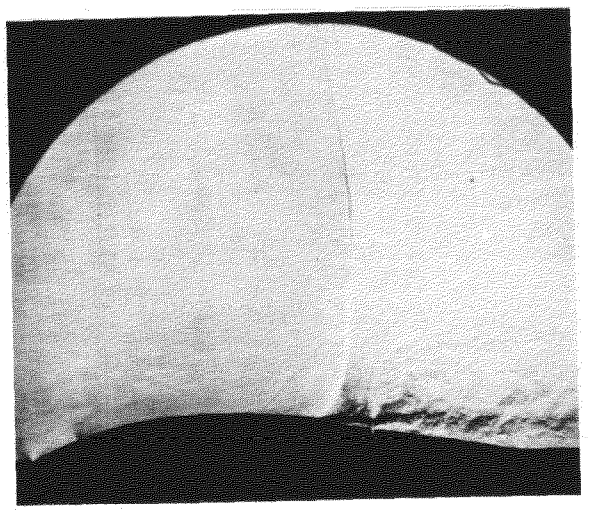

(b)

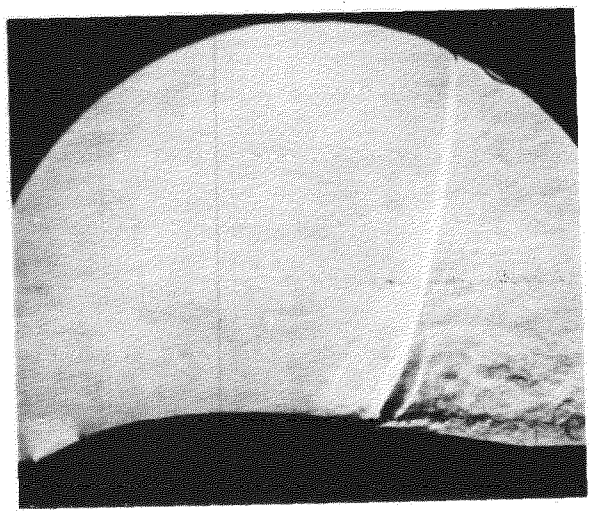

(c)

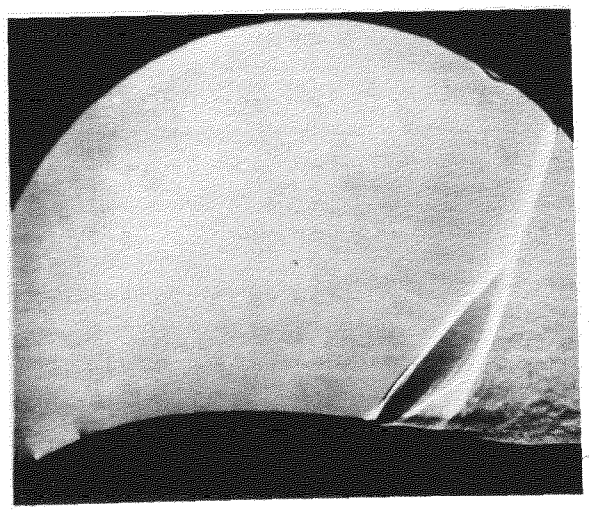

(d)

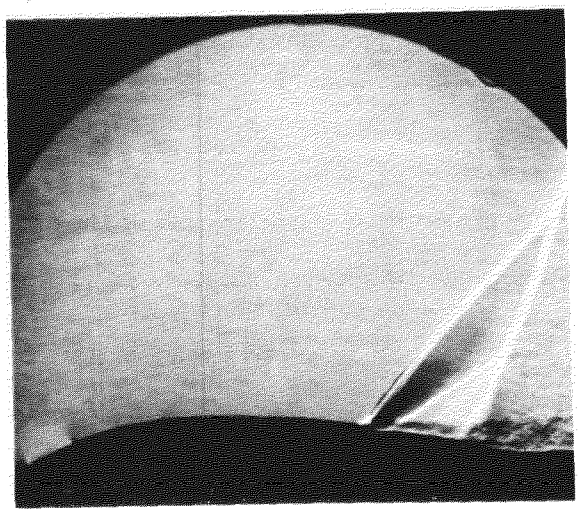

(e)

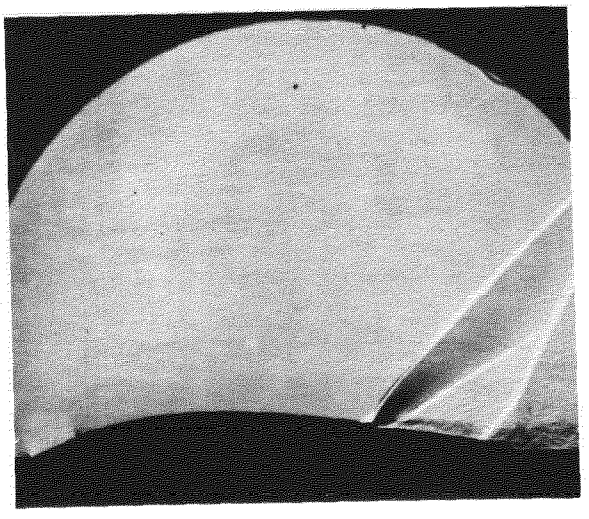

(f)

Schlieren photographs for the 8% thick bump. Blowing at 69·7% chord—40 p.s.i.

FIG. 29.

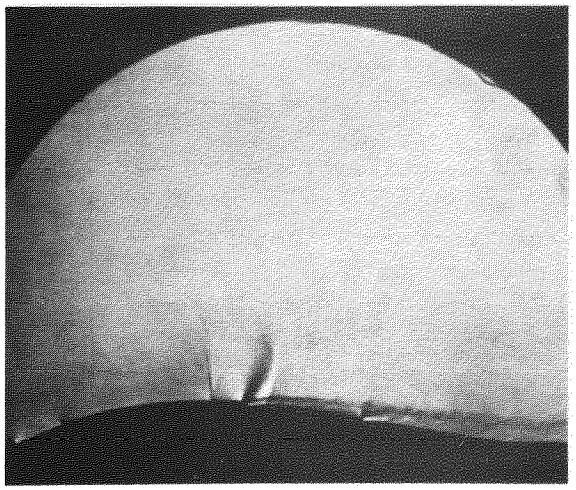

(a)

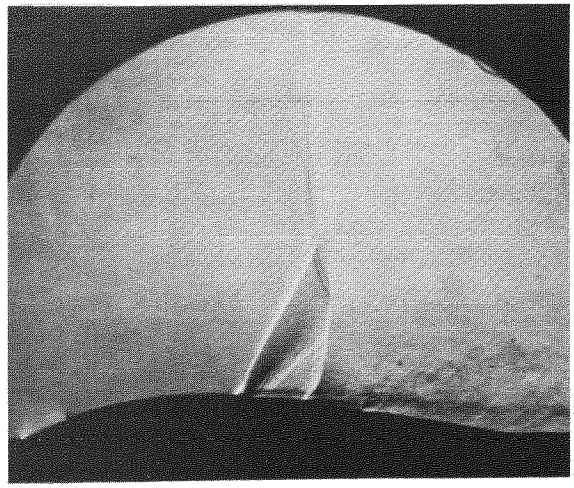

(b)

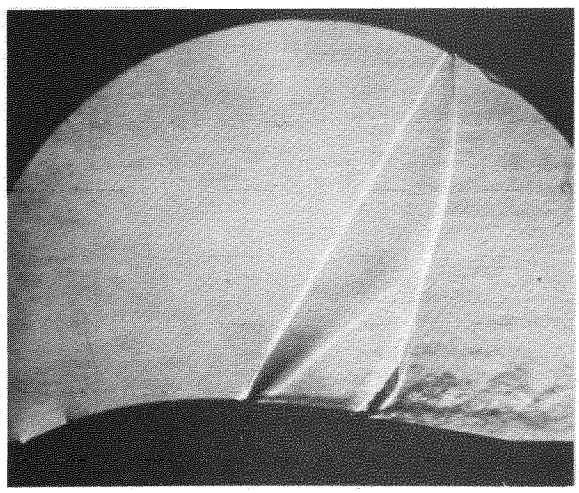

(c)

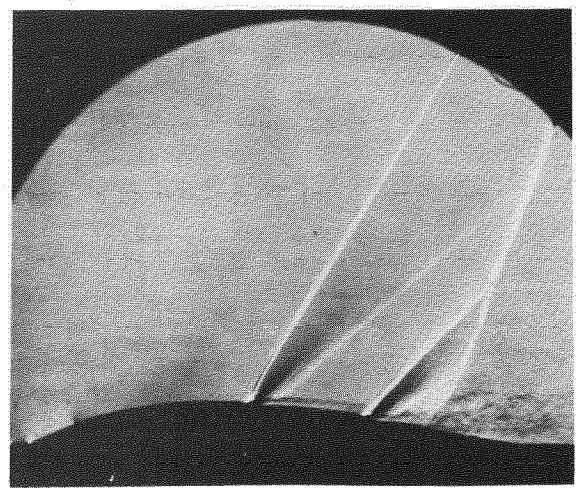

(d)

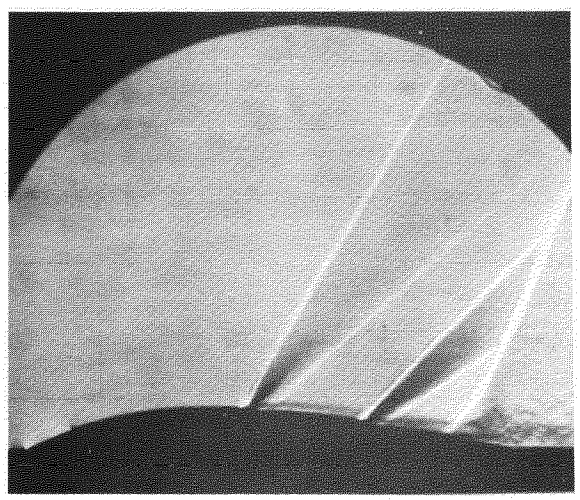

(e)

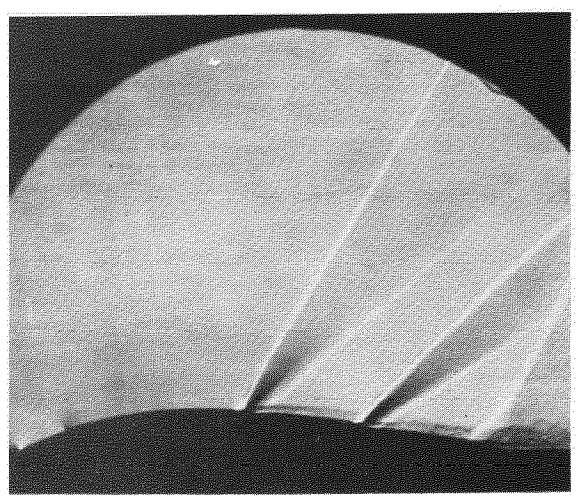

(f)

Schlieren photographs for the 8% thick bump.
Blowing at 45·5% and 69·7% chord—20p.s.i.

FIG. 30.

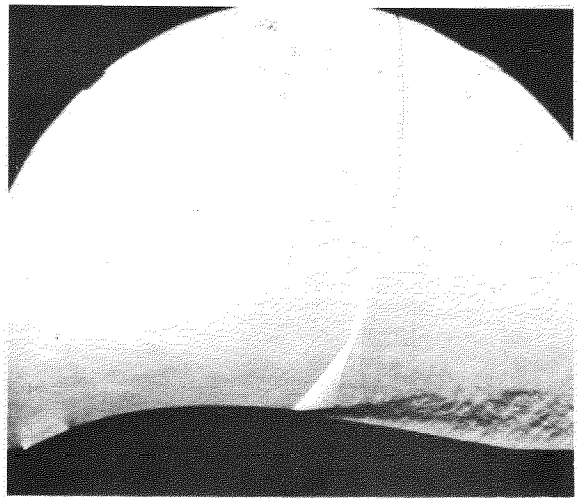

(a) No blowing

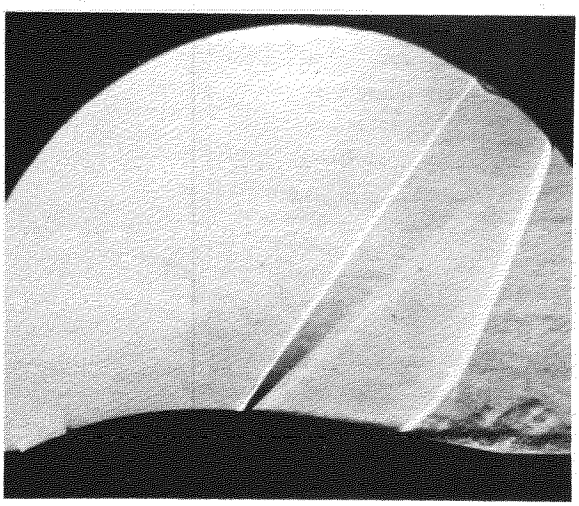

(b) 1 p.s.i. at 45·5% c.

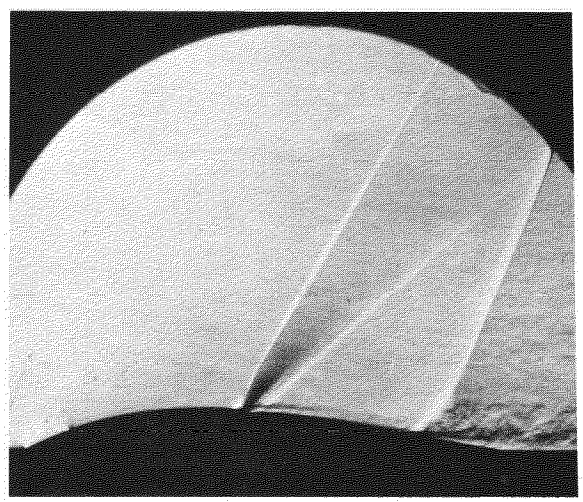

(c) 20 p.s.i. at 45 5% c.

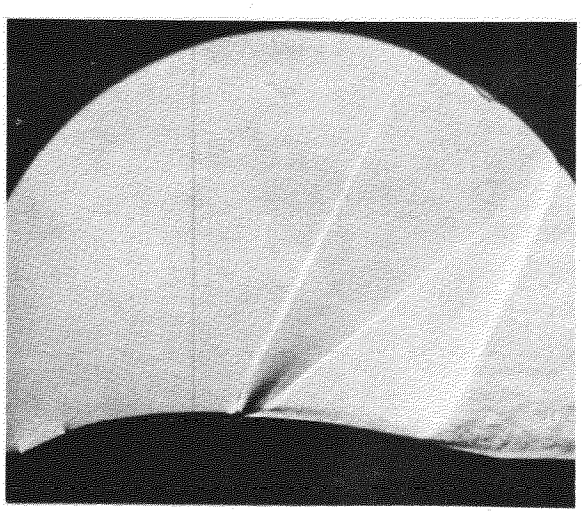

(d) 40 p.s.i. at 45·5% c.

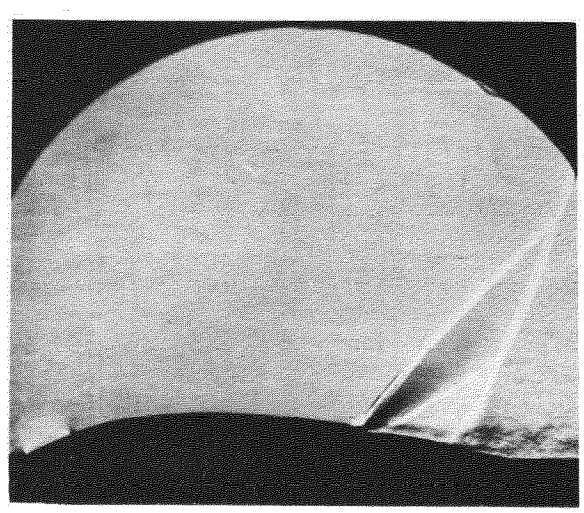

(e) 40 p.s.i. at 69·7% c.

FIG. 31.

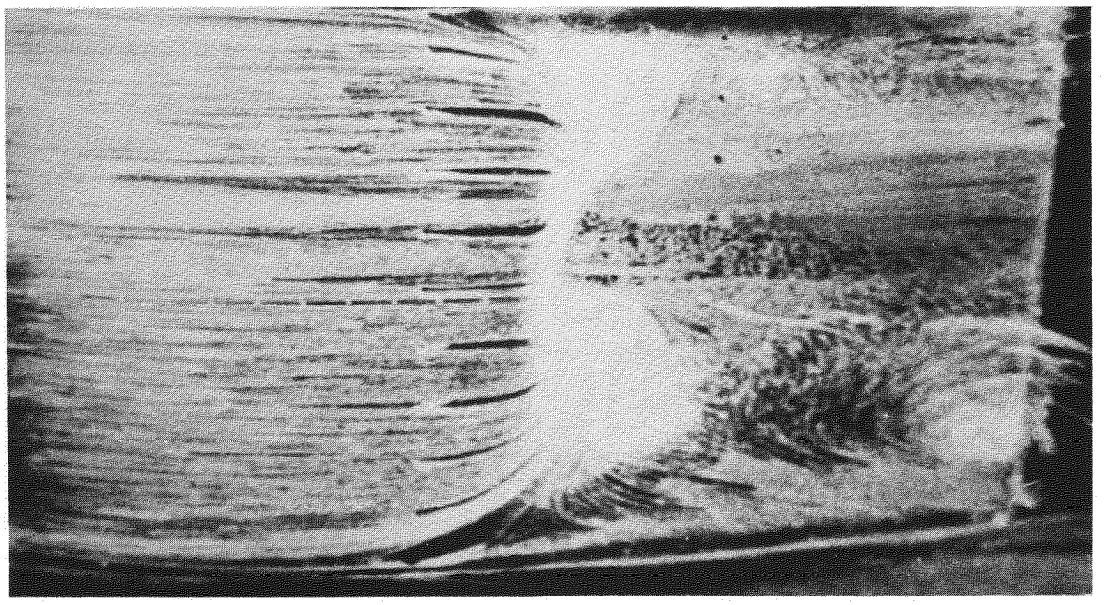

(a) No blowing.

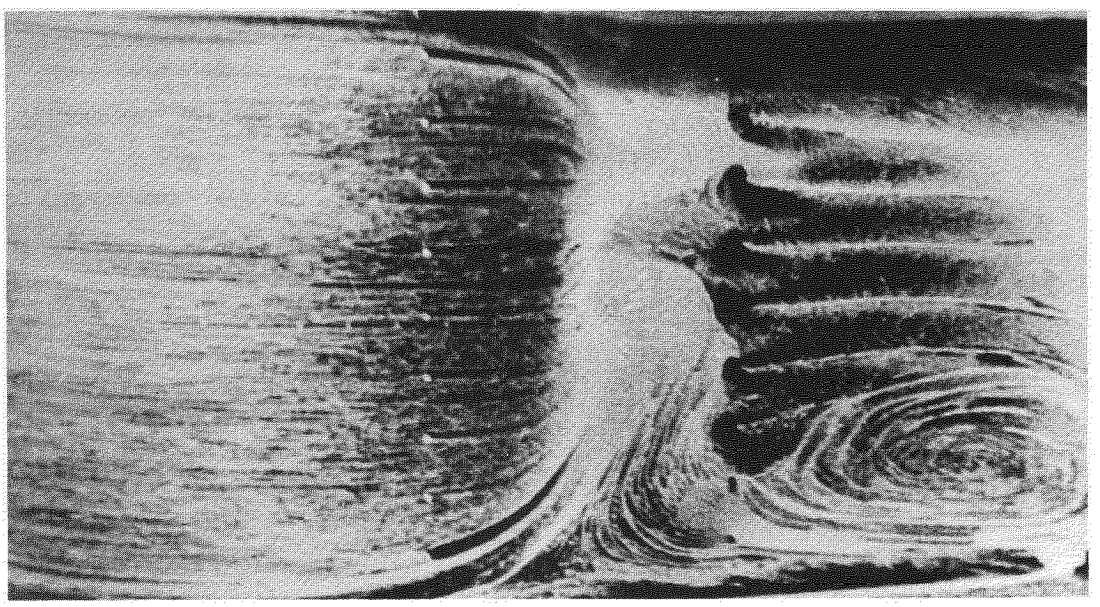

(b) 1 p.s.i. at 69·7% c.

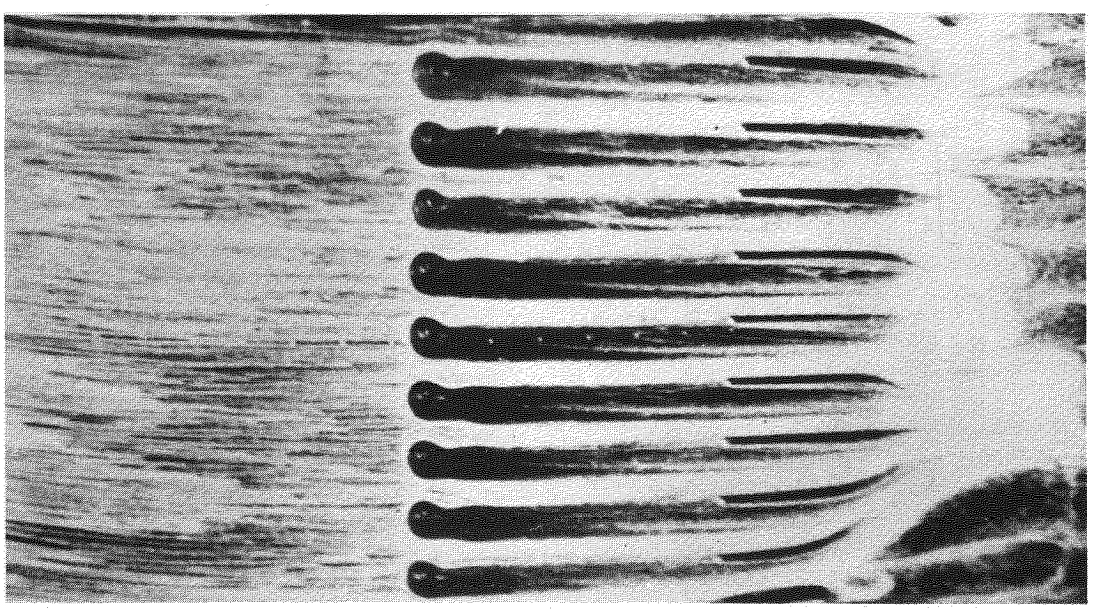

(c) 1 p.s.i. at 45·5% c.

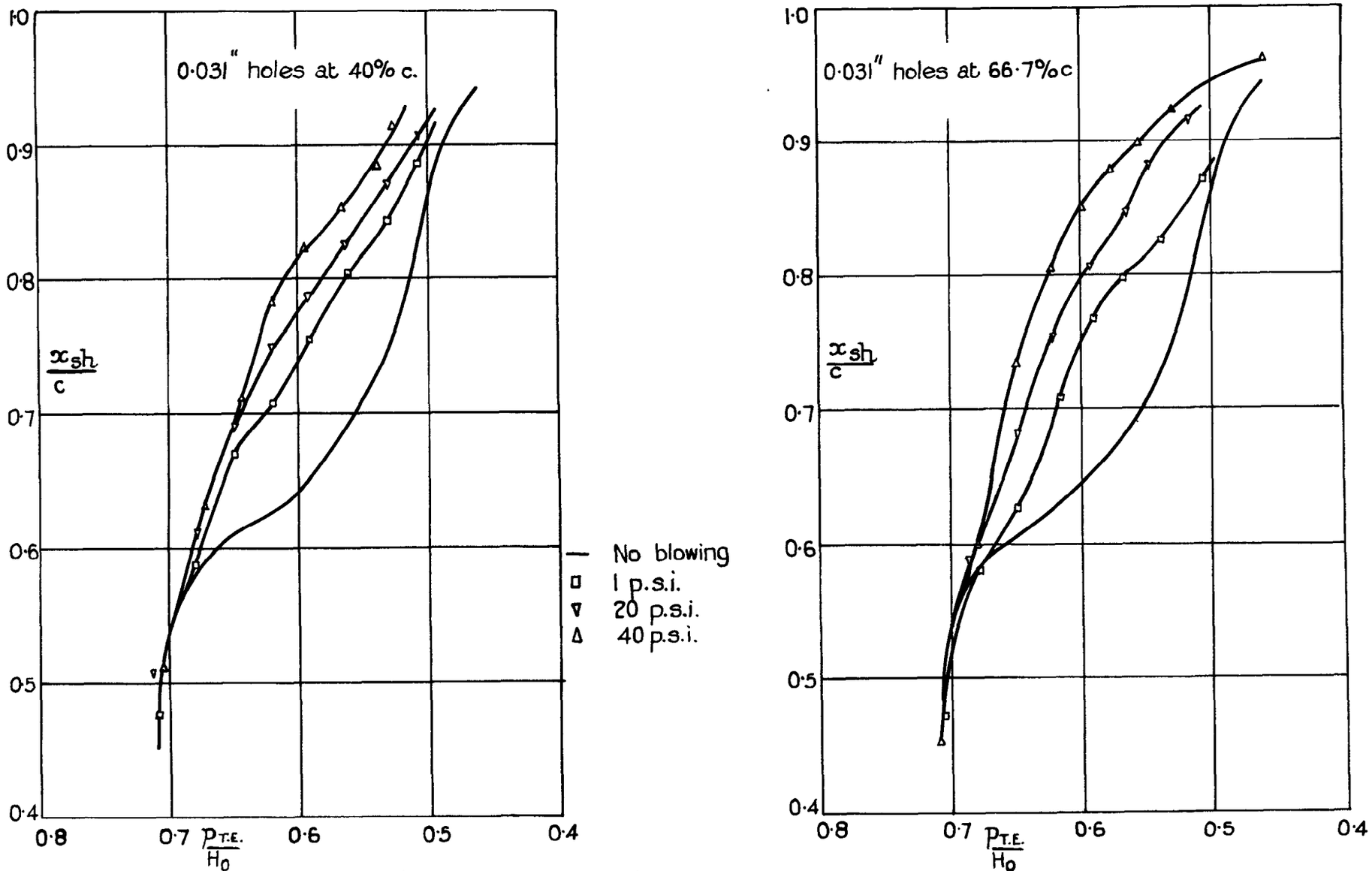

FIG. 32

Variation of shock position with trailing edge pressure for the 6% thick bump

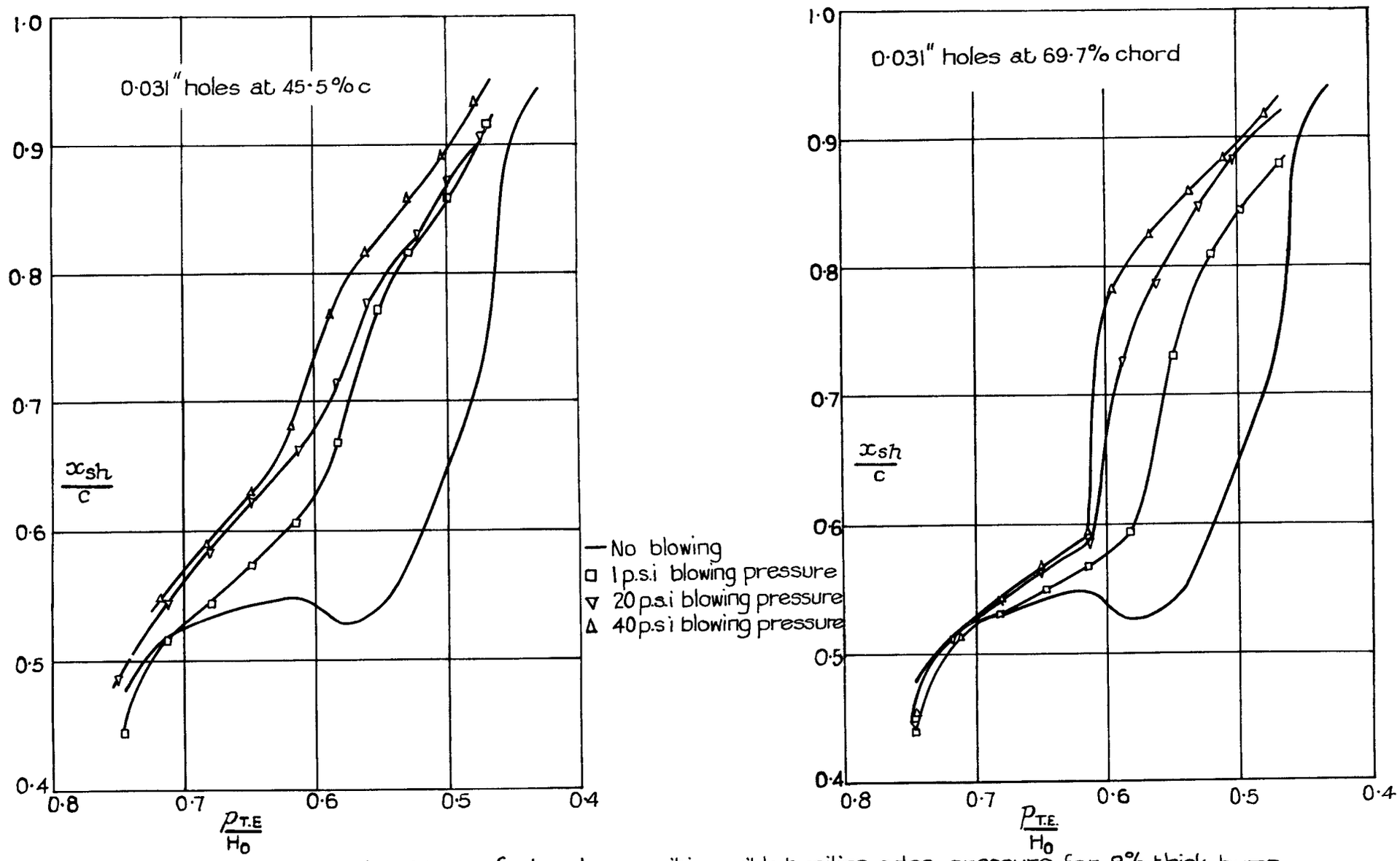

Variation of shock position with trailing edge pressure for 8% thick bump.

Fig. 33

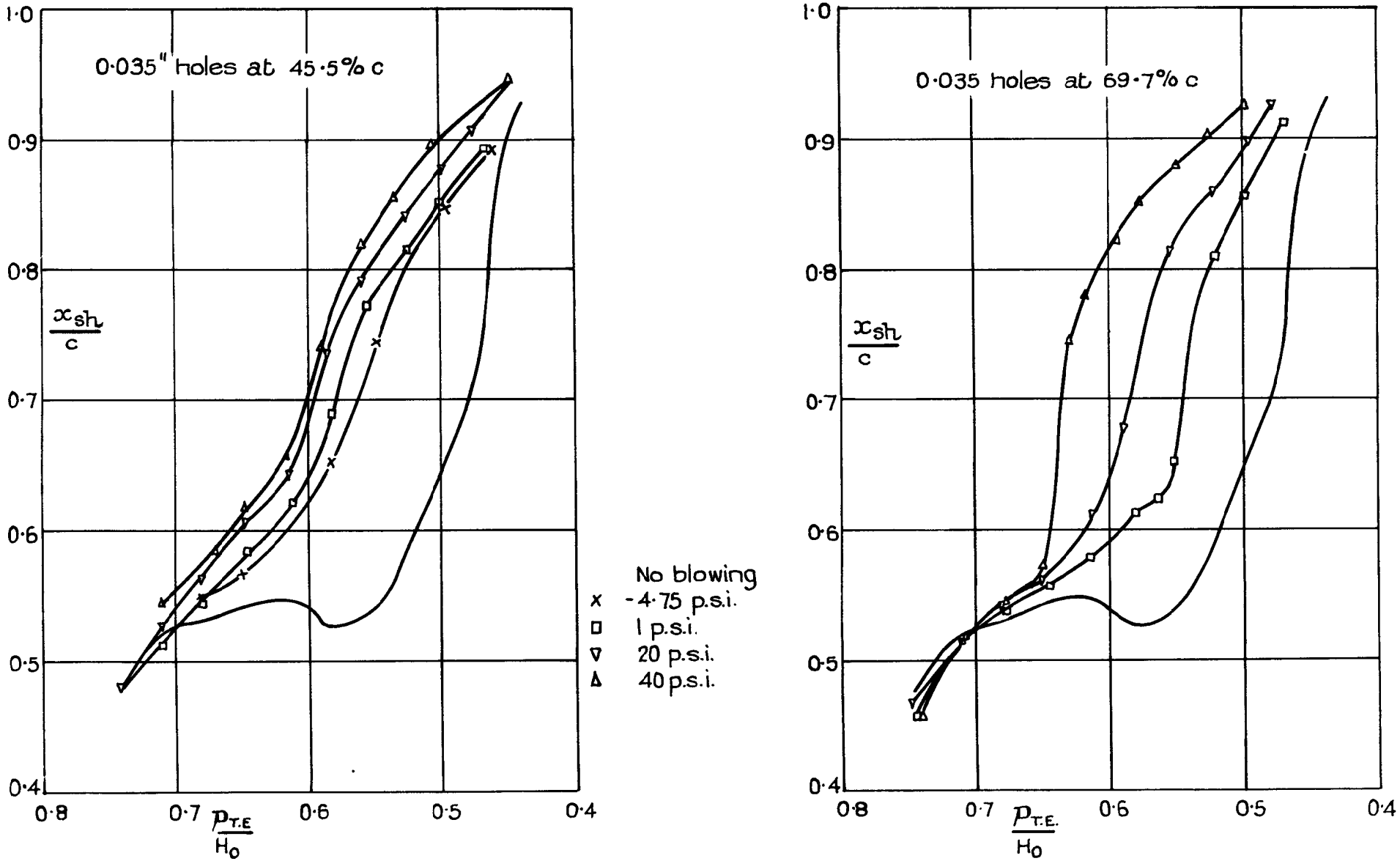

Variation of shock position with trailing edge pressure for 8% thick bump.

FIG. 34.

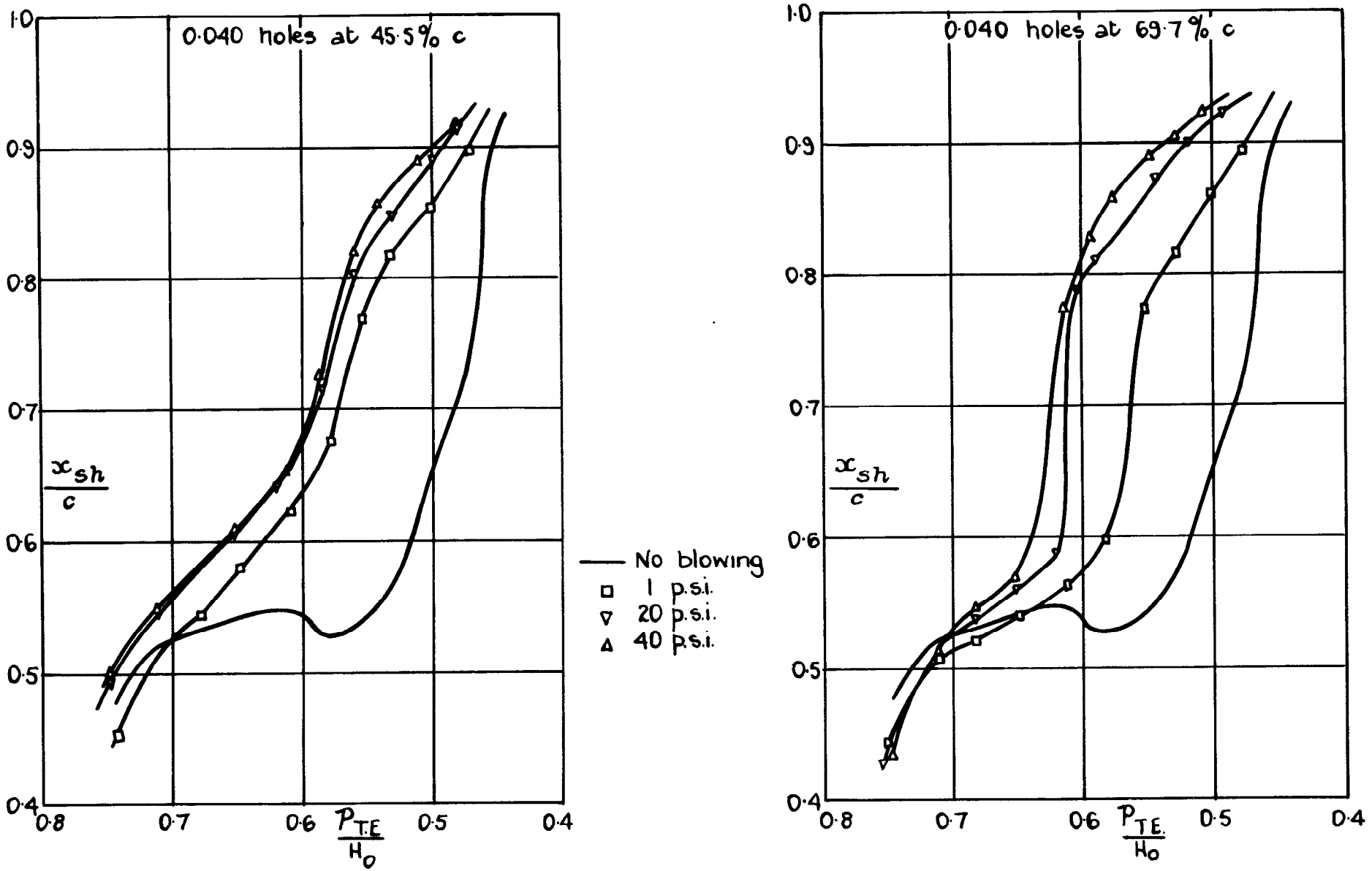

FIG. 35.

Variation of shock position with trailing edge pressure for 8% thick bump.

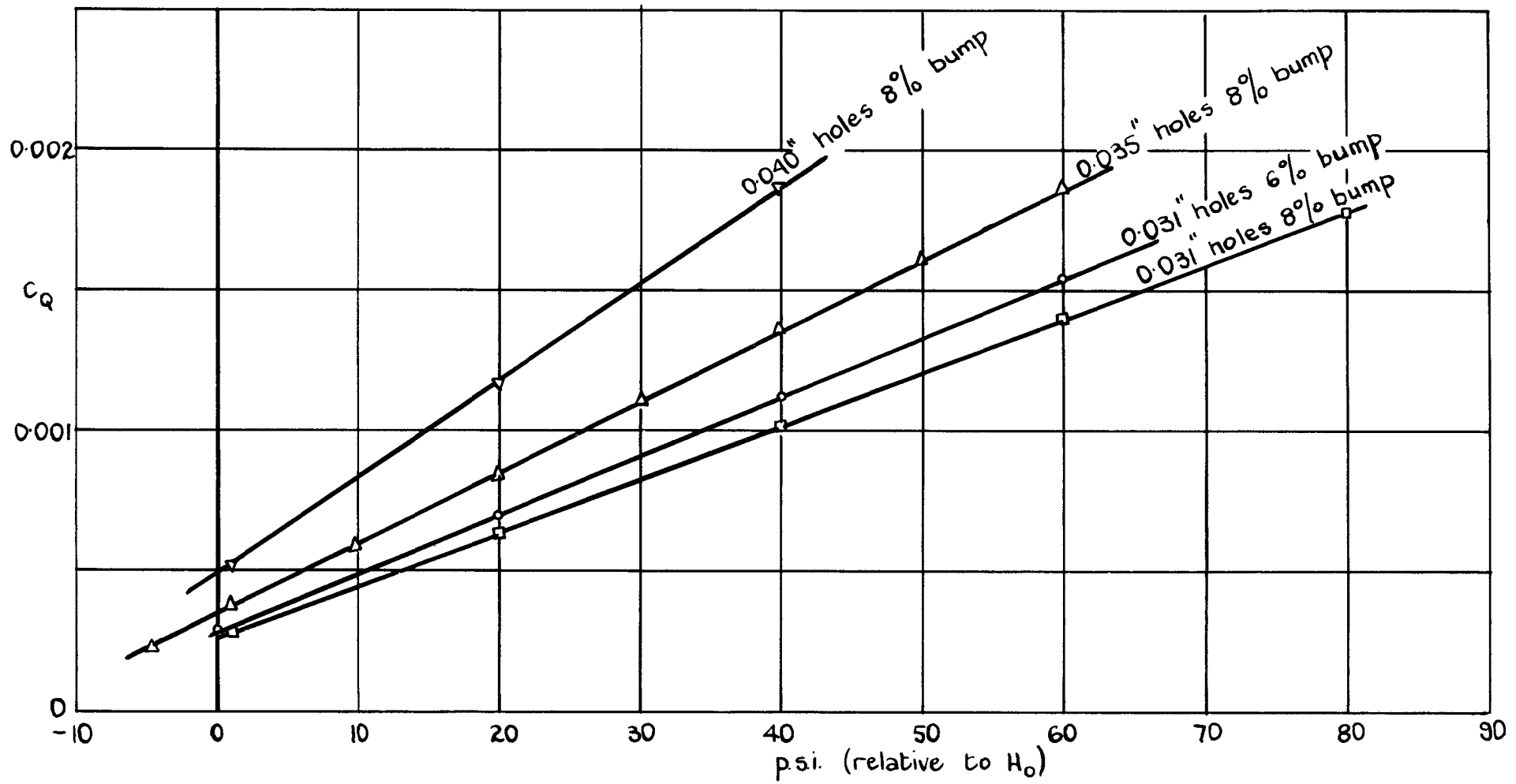

Variation of mass-flow coefficient (C_Q) with blowing pressure.

FIG 36.

FIG. 37.

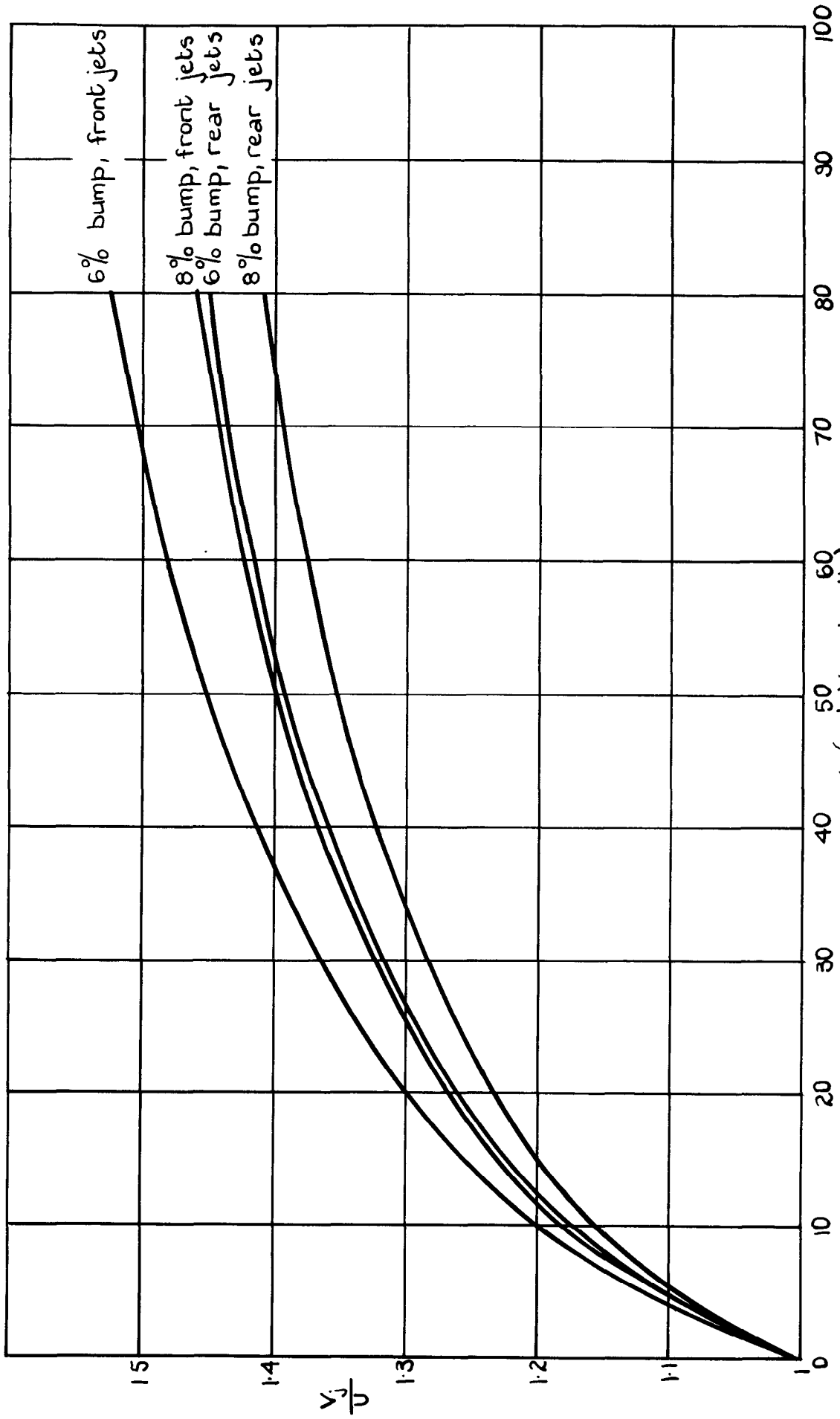

Variation of velocity ratio (jet velocity / local velocity) with blowing pressure

DS63929/1 W.5B K.4 5/62 CL

A.R.C. C.P. No.595
February, 1958
Wallis, R. A., Dept. of Supply, Australia, and
Stuart, Mrs. C. M., Nat. Phys. Lab.

ON THE CONTROL OF SHOCK-INDUCED BOUNDARY-LAYER SEPARATION WITH DISCRETE AIR JETS

Tests carried out on a half aerofoil fitted to the wall of a high-speed wind tunnel show that discrete air jets, possessing a spanwise ejection velocity, produce persistent vorticity and may be used to facilitate re-attachment of separated layers and, in some cases, almost to suppress separation.

A.R.C. C.P. No.595
February, 1958
Wallis, R. A., Dept. of Supply, Australia, and
Stuart, Mrs. C. M., Nat. Phys. Lab.

ON THE CONTROL OF SHOCK-INDUCED BOUNDARY-LAYER SEPARATION WITH DISCRETE AIR JETS

Tests carried out on a half aerofoil fitted to the wall of a high-speed wind tunnel show that discrete air jets, possessing a spanwise ejection velocity, produce persistent vorticity and may be used to facilitate re-attachment of separated layers and, in some cases, almost to suppress separation.

A.R.C. C.P. No.595
February, 1958
Wallis, R. A., Dept. of Supply, Australia, and
Stuart, Mrs. C. M., Nat. Phys. Lab.

ON THE CONTROL OF SHOCK-INDUCED BOUNDARY-LAYER SEPARATION WITH DISCRETE AIR JETS

Tests carried out on a half aerofoil fitted to the wall of a high-speed wind tunnel show that discrete air jets, possessing a spanwise ejection velocity, produce persistent vorticity and may be used to facilitate re-attachment of separated layers and, in some cases, almost to suppress separation.

Printed and published by
HER MAJESTY'S STATIONERY OFFICE

To be purchased from
York House, Kingsway, London, w.c.2
423 Oxford Street, London w.1
13A Castle Street, Edinburgh 2
109 St. Mary Street, Cardiff
39 King Street, Manchester 2
50 Fairfax Street, Bristol 1
35 Smallbrook, Ringway, Birmingham 5
80 Chichester Street, Belfast 1
or through any bookseller

Printed in England

S.O. Code No. 23-9012-95